Dynamic Determinants of Quorum Quenching Mechanism Shared among N-terminal Serine Hydrolases

Bartłomiej Surpeta,[†,‡] Michal Grulich,[§] Andrea Palyzová,[¥] Helena Marešová,[¥] and Jan Brezovsky[†,‡,]*

† Laboratory of Biomolecular Interactions and Transport, Department of Gene Expression, Institute of Molecular Biology and Biotechnology, Faculty of Biology, Adam Mickiewicz University, Uniwersytetu Poznanskiego 6, 61-614 Poznan, Poland

‡ International Institute of Molecular and Cell Biology in Warsaw, Ks Trojdena 4, 02-109 Warsaw, Poland

§ Laboratory of Modulation of Gene Expression, Institute of Microbiology,v.v.i., Academy of Sciences of the Czech Republic, Videnska 1083, 142 20 Prague 4, Czech Republic

¥ Laboratory of Molecular Structure Characterization, Institute of Microbiology,v.v.i., Academy of Sciences of the Czech Republic, Videnska 1083, 142 20 Prague 4, Czech Republic

*Email: janbre@amu.edu.pl

ABSTRACT

Due to the alarming global crisis of the growing microbial antibiotic resistance, investigation of alternative strategies to combat this issue has gained considerable momentum in the recent decade. A quorum quenching (QQ) process disrupts bacterial communication through so-called quorum sensing that enables bacteria to sense the cell density in the surrounding environment. Due to its indirect mode of action, QQ is believed to exert limited pressure on essential bacterial functions and consequently avoid inducing resistance. Although many enzymes are known to display the QQ activity towards various molecules used for bacterial signaling, the in-depth mechanism of their action is not well understood hampering their possible optimization for such exploitation. In this study, we compare the potential of three members of N-terminal serine hydrolases to degrade N-acyl homoserine lactones–signaling compounds employed by Gram-negative bacteria. Using molecular dynamics simulation of free enzymes and their complexes with two signaling molecules of different lengths, followed by quantum mechanics/molecular mechanics molecular dynamics simulation of their initial catalytic steps, we explored molecular details behind their QQ activities. We observed that all three enzymes

1

were able to degrade bacterial signaling molecules following an analogous reaction mechanism. For the two investigated penicillin G acylases from *Escherichia coli* (ecPGA) and *Achromobacter spp.* (aPGA), we confirmed their putative activities experimentally hereby extending the set of known quorum quenching enzymes by these representatives of biotechnologically well-optimized enzymes. Interestingly, we detected enzyme- and substrate-depended differences among the three enzymes caused primarily by the distinct structure and dynamics of acyl-binding cavities. As a consequence, the first reaction step catalyzed by ecPGA with a longer substrate exhibited an elevated energy barrier due to a too shallow acyl-binding site incapable of accomodating this molecule in a required configuration. Conversely, unfavorable energetics on both reaction steps were observed for aPGA in complex with both substrates, conditioned primarily by the increased dynamics of the residues gating the entrance to the acyl-binding cavity. Finally, the energy barriers of the second reaction step catalyzed by *Pseudomonas aeruginosa* acyl-homoserine lactone acylase with both substrates were higher than in the other two enzymes due to distinct positioning of Arg297β. These discovered dynamic determinants constitute valuable guidance for further research towards designing robust QQ agents capable of selectively controlling the virulence of resistant bacteria species.

INTRODUCTION

Efficient control of bacterial populations is critical for various aspects of our daily life. In the past decades, the application of antibiotics constituted the primary strategy to address this challenge in human and veterinary medicine, animal food production, agriculture, aquaculture, or as anti-biofouling agents in various industries and remain as such for most of these fields.[1–6] Unfortunately, the interference of antibiotics with the essential bacterial functions exert high selective pressure, which results in the development of antibiotic resistance via numerous distinct mechanisms.[6] A widespread misuse and overuse of antibiotics in almost all of their application fields further fuels the development of resistance.[7–11] Above and beyond, the recent studies show that the resistance genes can be transferred between bacteria of the same, or even different species, enabling the spread of resistance without direct exposure to antimicrobials.[12,13] As a result, resistant bacteria have been detected in all examined environments including soil, sea, food products, drinking water or even samples from Antarctica.[12,14–17] Overall, the spiraling antibiotics resistance constitutes an alarming global crisis.[7,8,18,19]

To address these threats and keep up with rapidly evolving antibiotics resistance,[6,12,17,20] considerable effort must be made cooperatively on the global scale to cope with this

progressing crisis efficiently.[8] First of all, the emergence of resistance towards currently used antibiotics can be delayed by the extensive education on this problem to increase social awareness, improved diagnosis, appropriate prescriptions, and limiting the use of antibiotics in agriculture, aquaculture, to preserve the priority of the most efficient antimicrobials usage for medication only.[8,12,21–24] Simultaneously, the discovery and development of new generations of antimicrobials as an alternative to currently available and widely used conventional antibiotics would help with the widespread alarming bacterial resistance. Nevertheless, methods employed for searching for new drugs were not overly successful in offering solutions to keep up with immensely progressing resistance development in past decades.[25–28] This is conditioned chiefly by multiple bacterial mechanisms to avoid the toxicity of the active compounds including penetration barriers, strategies focused on the antibiotic inactivation by their destruction, modification and/or excretion with efflux pumps or those concentrated on the target modification, switching or sequestration.[26,29,30] Therefore, in the long run, alternative strategies targeting non-essential bacterial functions, which reduce the pressure on resistance development, are needed to complement or even substitute antibiotics usage at least in some of their application fields.[31–35]

Bacterial virulence factors constitute a promising target for such new strategies, which aim at disarming rather than killing bacteria. One of the most extensively studied approaches is disrupting the quorum sensing (QS) process. QS allows communication between bacteria and results in collective behavior in a population density-depended manner controlled by the concentration of specific signaling molecules.[36,37] These molecules bind to transcriptional activators and stimulate the expression of genes responsible for the regulation of virulence factors, production of secondary metabolites, formation of biofilms, and other components crucial for their pathogenicity.[38] The disruption of QS, widely known as quorum quenching (QQ), was already shown to be a promising strategy for anti-biofouling,[39] treatment of bacterial infections[40] and protection of crops or aquacultures.[36,41]

Various types of organic molecules were described to play a role in QS depending on the bacterial species, including N-acyl-homoserine lactones (HSLs)[41] which are predominantly used by highly pathogenic Gram-negative bacteria, such as one of the critical priority species– *Pseudomonas*.[42] For example, the QS signal in the globally prioritized *Pseudomonas aeruginosa* is carried by N-(3-oxo-dodecanoyl)-L-homoserine lactone. In this case and analogously in other species,[43] QQ can be achieved by inhibiting either HSL signal synthesis performed by LasI protein and/or signal detection by LasR protein which is a transcriptional activator of the QS genes.[37,43] Although the application of quorum sensing inhibition (QSI) can

effectively interfere with bacterial communication, it is not entirely escaping the development of resistance against QSI by altering the structure of protein targets or via the action of efflux pumps as already shown for furanone C-30 in *P. aeruginosa*.[43–45] In this view, the direct inactivation of signaling compounds[37,46] by the action of QQ enzymes is less likely to exert pressure on bacteria by operating out-of-cell, on the environmental level, and hence avoids the development of the resistance by mechanisms known for antibiotics, drugs, or QSI.[36]

Up to date, three classes of enzymes capable of QQ the HSL-based communication have been discovered: (i) acylases (amidases) which cleave the amide bond between the homoserine lactone and acyl chain, (ii) lactonases which breaks the lactone ring, and (iii) oxidoreductases which modify the acyl chain.[36,37,41] HSL degradation performed by acylases is irreversible, while their cleavage products are neutral and easy to metabolize. Furthermore, in contrast to the other two classes of QQ enzymes, acylases are often specific towards a narrow range of signaling molecules, which allows for the selective targeting of pathogenic microbes and avoiding undesired side effects on the beneficial microbiota,[39] and escaping from the compromised efficiency of broadly active enzymes exposed for multiple targets.[47] Most QQ acylases belong to the N-terminal hydrolase superfamily, sharing common features including auto-proteolytic activation by cleavage of linker peptide and the activity based on N-terminal residue–serine, threonine or cysteine–acting as a nucleophile in the enzyme self-activation and further function. They are classified into four main subfamilies: aculeacin A acylase, penicillin G acylase, AmiE amidase or penicillin V acylase.[37]

Pseudomonas aeruginosa acyl-homoserine lactone acylase (paPvdQ) from aculeacin A acylase subfamily is the most developed acylase in terms of its practical QQ application. paPvdQ preferentially cleaves long HSLs (~12 carbon atoms) as conditioned by a deep acyl-binding cavity (**Figure 1A**).[48] By breaching this cavity, Koch *et al.* successfully altered the specificity of paPvdQ towards C08-HSL signaling molecule used by *Burkholderia cenocepacia*, enabling host survival in *Galleria mellonella* infection model.[49] Moreover, a dry powder formulation of this protein was developed for *Pseudomonas aeruginosa* pulmonary infection treatment by inhalation,[50] recently shown to be effective in vivo using a mouse model.[40] Although these applications render paPvdQ a promising QQ agent, the molecular mechanism of its action is not fully understood, restricting its further development.
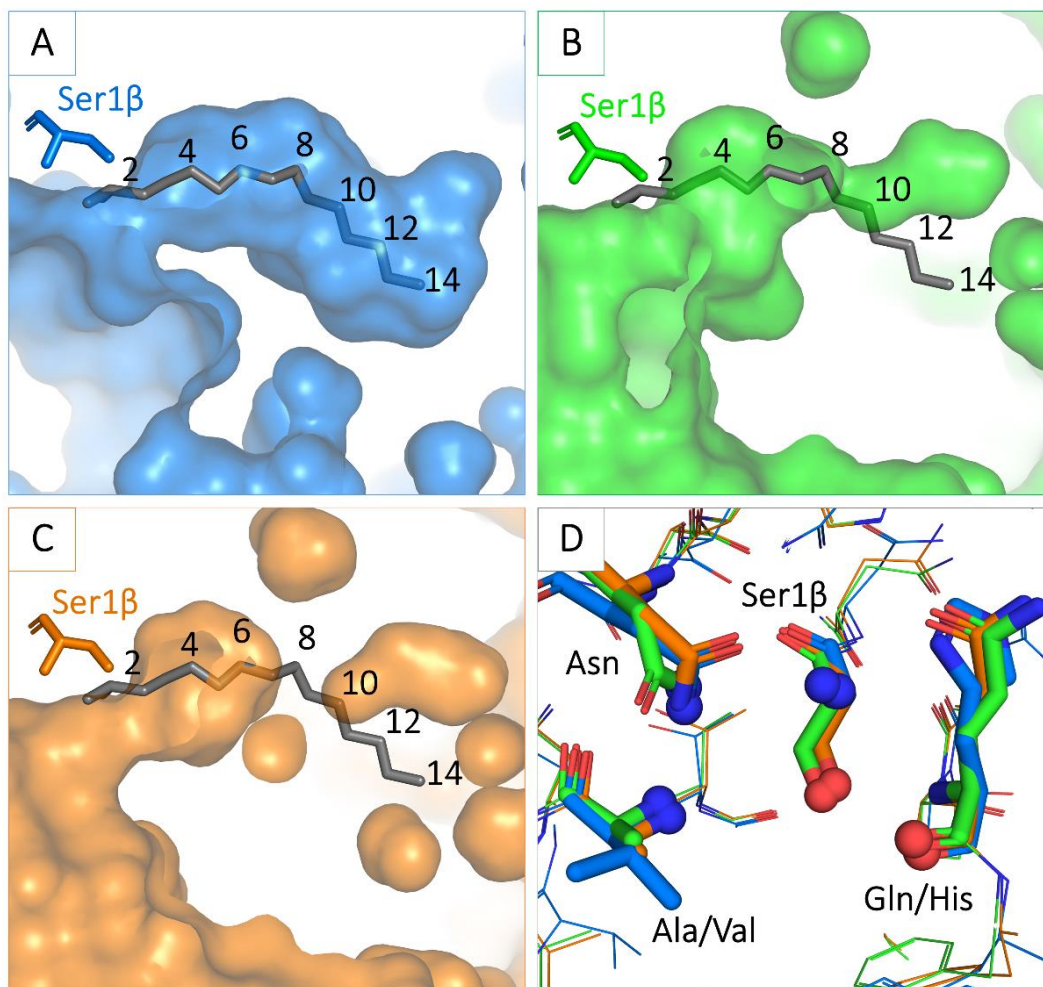
Figure 1. Structural prerequisites for quorum quenching activity among N-terminal serine hydrolases. Geometries of substrate binding pockets in crystal structures of A) paPvdQ (PDB-ID: 4M1J), B) kcPGA (PDB-ID: 4PEL), and C) ecPGA (PDB-ID: 1GK9). D) Conserved positioning of functional groups in catalytic residues across all three enzymes. Gray sticks in A-C represent transition state analog of the paPvdQ's, highlighting its acyl-binding subpocket suitable for binding long-chain HSLs. The same analog superimposed into PGAs structures indicates the possibility to accommodate HSLs of up to 8 carbon atoms.

Recently, *Kluyvera citrophila* penicillin G acylase (kcPGA) was shown to display QQ activity towards short HSLs consistently with a significantly shallower acyl-binding cavity observed in the crystal structure compared to paPvdQ (**Figure 1B**).[51] However, other PGAs that share a high level of sequence and structure similarity to kcPGA (**Figure S1, Table S1**), including very well characterized *Escherichia coli* PGA (ecPGA, **Figure 1C**), had not exhibited any appreciable QQ activity.[52] Since all three enzymes, ecPGA, kcPGA, and paPvdQ, are equipped with equivalently placed functional groups responsible for their catalytic action (**Figure 1D**), it is believed that the observed differences in their activity arise from differences in their functional dynamics.[51,53,54]

5

To uncover unknown determinants governing the QQ activity catalyzed by N-terminal serine hydrolases, our study focuses on the role of dynamics in the molecular function of prototypical paPvdQ and related yet inactive ecPGA employed as the negative control. By contrasting the plasticity and pre-organization of their active site residues, their ability to stabilize productive binding modes of substrates, and atomistic details of their reaction mechanisms, we have revealed crucial structure-dynamics-functions relationships relevant for the future discovery and design of robust enzyme-based QQ agents competent to substitute or support antibiotics and selectively combat resistant bacteria species.

METHODS

A full description of simulation details and system setup is available in the Supporting Information.

Molecular dynamics of free enzymes. Crystal structures of ecPGA (PDB-ID: 1GK9) and paPvdQ (PDB-ID: 4M1J) were obtained from the PDB database.[55,56] For *Achromobacter spp.* penicillin G acylase (aPGA), a previously derived homology model was retrieved from Protein Model Database (ID: PM0080082)[57] and corrected using RepairPDB module of FoldX.[58] Structures were protonated with H++ webserver[59–61] at pH 7.5 using the default salinity, internal and external dielectric constants. Protonated structures, including crystallographic waters, were placed in a truncated octahedron box of TIP3P waters with a distance of 10 Å from any atom in the structure and neutralized using Na+ and Cl- ions to approximately 0.1 M concentration. Initial parameters and topologies were generated using tleap module of AmberTools17.[62] System hydrogen atom masses were repartitioned to enable 4fs time-step during simulations with SHAKE algorithm.[63,64] Energy minimization and molecular dynamics (MD) simulations were performed using ff14SB force field[65] by pmemd and pmemd.CUDA modules of Amber16 package, respectively.[62] The systems were energy minimized, equilibrated, followed by 500 ns of NPT production MD simulations at 310 K with Langevin thermostat.[66] All steps were performed in triplicates to generate three independent replicas. The stability of the production phase was inspected in terms of root-mean-square deviation (RMSD) of the backbone heavy atoms (**Figure S3 and S20**).

Free enzyme dynamics analysis. The opening of the acyl-binding cavity across free enzyme MD trajectories was explored by CAVER 3.0.2 software.[67] The starting point for the calculation of paths was specified based on the center of mass of three residues–Met142α, Ser67β, Ile177β for PGAs, and Leu146α, Leu53β, Trp162β for paPvdQ.[49] Potential acyl-binding site opening events were identified using a probe radius of 0.5 Å. The time sparsity 10

was used to reduce the computational cost of this analysis. The paths were clustered using a threshold of 3.5, and one representative was selected for each cluster.

Cpptraj module of AmberTools17 was used to measure relevant distances across all MD trajectories between functional atoms in the catalytic residues. Further, the network of distances was subjected for dimensionality reduction using the principal component analysis (PCA) implemented in scikit-learn Python library.[68]

Receptor selection and molecular docking. Protein conformations harboring spatially well-shaped acyl-binding cavities and favorably pre-organized catalytic machinery were selected as receptor structures for ligand docking according to the criteria presented in **Table S2** "*receptor selection for docking*". These criteria were employed to promote proper orientation of the hydroxyl hydrogen of nucleophile serine to its amine group acting as a hydrogen acceptor in the first reaction step and provide properly pre-organized catalytic machinery, i.e., nucleophile serine and oxyanion hole stabilizing residues, for reactive binding of substrate.[53,57,69,70]

Molecular docking of C06- and C08-HSLs was performed using Autodock4.2.6,[71] Representative protein-ligand complexes were selected for the following round of simulations based on the mechanism-based selection criteria[72], as listed in **Table S2** "*selection of complexes for MDs*" to guarantee acceptable nucleophile distance and proper stabilization of the oxyanion hole, and their favorable Autodock binding score.

Molecular dynamics of protein-ligand complexes. Systems were prepared analogously to the free enzyme simulations using tleap and Parmed modules of AmberTools18.[73] Minimization and equilibration were performed using the same protocols as described for free enzyme simulations with the additional restraints on the ligand molecule. 50 ns of unrestrained NPT production simulations were performed in 310 K, using Langevin thermostat. All ligand-protein simulations, including minimization, equilibration, and production runs, were performed in 15 independent replicas. The stability of the production runs was inspected in terms of the protein backbone heavy atoms RMSD, analogously to free enzyme simulations (**Figure S4-S5** and **S21**) using Cpptraj module of AmberTools18.

Complexes binding free energy and ligand stabilization estimation. MMPBSA.py module of AmberTools18 package was used to estimate the binding free energy of the complexes using Molecular Mechanics / Generalized Born Surface Area (MM/GBSA).[74] Calculations were performed with Generalized Born implicit solvent model 8 at 0.1 M salt concentration. Per residue binding free energy decomposition was generated and results filtered to extract the most contributing residues, namely below -0.5 kcal/mol and above 0.5 kcal/mol for favorable and unfavorable contributions, respectively.

Quantum Mechanics/Molecular Mechanics MD simulations. (QM/MM MD) simulations were performed using sander module of Amber18 package. The initial frame for each protein-ligand complex was extracted from standard MD simulations by searching for the reactive-like configurations fulfilling the criteria listed in **Table S2** "*selection of representatives for sMDs*". Systems were equilibrated during 10 ns NPT simulation with the same settings as for protein-ligand production runs with additional 25 kcal mol^{-1} Å^{-2} harmonic restraints. Then, 500 ns production simulations were performed for each complex with distance restraints of the crucial interactions (**Table S2** "*restraints for sMDs inputs generation*"), collecting restart files resulting in an ensemble of 500 equivalent starting points per complex. Each starting conformation was equilibrated in QM/MM MD simulations maintaining the distance restraints (**Table S2** "*restraints for 1st QM/MM equilibration*"). The QM region composed of HSL molecule and the selected active site residues (**Figure S2**) was described with PM6-D semi-empirical method,[75–77] and the remaining part of the system was treated on MM level with ff14SB force field.

Further, steered QM/MM MD simulations of the acylation process were performed. This was divided into two steps: first, the tetrahedral intermediate (TI) formation, and the second, collapse of TI and acyl-enzyme (AE) formation. In the first step, the reaction coordinate (RC) was represented as a linear combination of distances (LCOD) involved in the proton transfer: d1(Ser1β-N-amine → Ser1β-H-hydroxyl) – d2(Ser1β-O-hydroxyl → Ser1β-H-hydroxyl) shown in **Figure 2A** simulated from 1.1 to -1.1 Å with harmonic restraint of 1000 kcal mol^{-1} Å^{-2}. Correctly formed TIs were equilibrated on the same level of theory as before, with the distance restraints for newly formed covalent bond (1.5 Å) and for the distance between closest nucleophile serine amine hydrogen to the amide nitrogen of the substrate which serves as a proton acceptor in the next step of the reaction (2.0 Å), as shown in **Table S2** "*restraints for 2nd QM/MM equilibration*".

Successfully equilibrated TIs were used as starting points for the second step of the acylation reaction. Here, RC was represented as LCOD involved in the AE formation: d3(HSL-C-carbonyl → HSL-N-amide) – d4(HSL-N-amide → Ser1β-NH-amine(closest)) + d5(Ser1β-N-amide → Ser1β-NH-amine) presented in **Figure 2B**, simulated from 0.6 to 4.9 Å with harmonic restraint of 1000 kcal mol^{-1} Å^{-2}. Work calculated from these verified simulations served as inputs to calculate the potential of mean force (PMF) profiles using Jarzynski's equality.[78] Errors in PMF profiles were estimated using a block-averaging scheme.
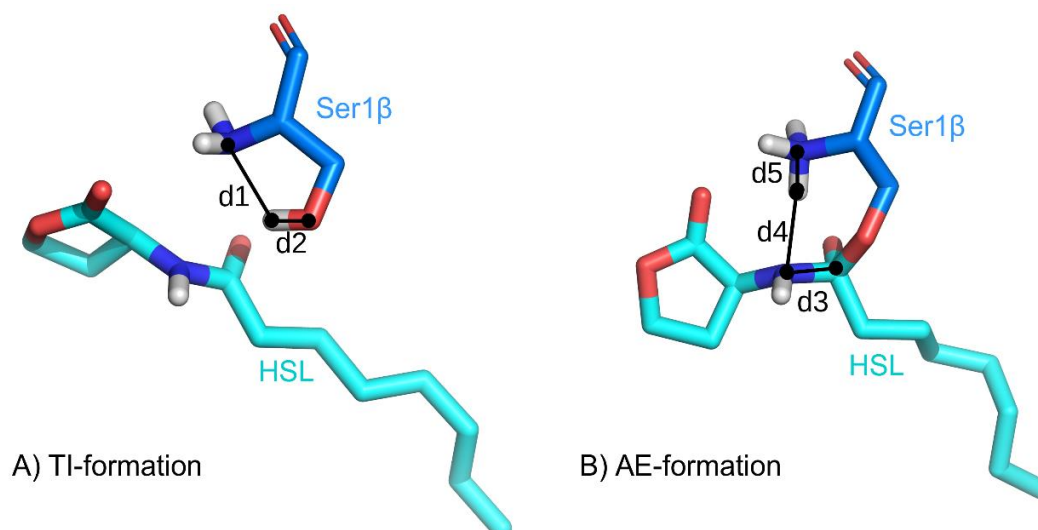
Figure 2. Linear combination of distances (LCOD) representing the reaction coordinate on two steps of steered MD simulation of HSL acylation. A) LCOD for tetrahedral intermediate formation composed of the distance of the transferred hydrogen to amine nitrogen distance and the distance of the same hydrogen to hydroxyl oxygen (d1-d2, steered from 1.1 to -1.1 Å). B) LCOD used at the second step of acylation resulting in acyl-enzyme formation, including the distance of the substrate amide bond, transferred hydrogen to the substrate leaving nitrogen and the same hydrogen to serine amine nitrogen (d3-d4+d5, steered from 0.6 to 4.9 Å).

Microorganisms and culture conditions. The production recombinant strains *E.coli* RE3(pKA18)[79] and *E. coli* BL21(pKX1P1)[80] growing in a stirred bioreactor as a fed-batch culture were used in this study to prepare biomass for purification of ecPGA and aPGA. The cultivations were carried out in a bioreactor Biostat MD (B. Braun Biotech Int., Melsungen, Germany) with the working volume of 6 l at 28 °C for 24 h. Both strains were cultivated in a defined medium M9 (0.4 % $(NH_4)_2SO_4$, 1.36 % KH_2PO_4, 0.3 % NaOH, 0.2 % $MgSO_4 \cdot 7H_2O$, 0.02 % $CaCl_2 \cdot 6H_2O$, 0.01 % $FeSO_4 \cdot 7H_2O$, pH 7.2) supplemented with glycerol (10 g/l) and casein hydrolysate (10 g/l) as the carbon and energy sources for the strain *E. coli* BL21 (pKX1P1) and sucrose (10 g/l) for the strain *E. coli* RE3(pKA18). The solution of 40% glycerol was used for feeding of *E. coli* BL21 (pKX1P1) and 50% sucrose for feeding of *E. coli* RE3(pKA18) when the concentration of carbon sources in the bioreactor dropped to zero. The fermentation operating parameters were set as initial stirrer speed 300 rpm, airflow rate 1 vvm and pH 6.5 was maintained by 25% NH_4OH. A concentration of dissolved oxygen (pO_2) was maintained at 20% of the value of air saturated medium by cascade regulation of stirring frequency in the course of the initial batch phase of the culture. During the fed-batch phase, the stirring was set up to 800 rpm and the feeding was controlled by the value of the dissolved oxygen (pO_2 of 20%). The culture from 200 ml of minimal medium M9 grown for 16 h at 28 °C was used as inoculum.

9

Enzyme purification and hydrolytic activity assay. aPGA was purified as described by Škrob *et al.*[81,82] and ecPGA according to Kutzbach and Rauenbusch.[83] The activity of 1 unit (U) was defined as the amount of aPGA or ecPGA cleaving 1 μmol of corresponding HSL per min in 0.05 M sodium phosphate buffer at pH 8.0 and 7.0, respectively, containing 2 % (w/v) HSL at 35 °C. All HSLs were obtained from Sigma-Aldrich co.

Effect of pH and temperature on activity of PGAs. The temperature optimum for activity was determined in the range of temperatures from 30 °C to 70 °C in 0.05 M phosphate buffer at pH from 5.0 to 8.0 for both studied HSL signaling molecules. In case of the ecPGA enzyme, the maximum activity was observed at 35-40°C at pH 7.0, whereas the maximum of activity of aPGA was observed at 50 °C and pH 8.0.

Contribution of autohydrolysis to activity of PGAs. Stability of C06-HSL was evaluated to estimate the extent of substrate autohydrolysis occuring during the enzymatic reaction, at the following substrate concentrations: 5, 10, and 20 mM in 0.05 M phosphate buffer at pH 7 and temperature of 35°C.

Enzyme kinetics. Kinetic characterization of HSL degradation by ecPGA and aPGA was carried out in 0.05 M phosphate buffer at pH 7.0 and 8.0, respectively and at temperature optimum for ecPGA (35°C). Concentrations of reactants were monitored by HPLC. The aliquotes were adjusted at pH 2 in order to stop the reaction and evaporated to dryness at 35°C. Residues were dissolved in 0.2 mL of HPLC grade acetonitrile. 20 μL of acetonitrile solutions were applied onto an analytical RP-C18 HPLC column (250 x 4.6, 5 μm particle size (Hypersil ODS)). The elution procedure consisted of an isocratic profile of methanol-water (50:50, v/v) for 10 minutes, followed by the linear gradient from 50 to 90 % methanol in water over 15 minutes, and an isocratic profile over 25 minutes. The flow rate was 0.4 mL/min and monitored at 210 nm. Retention times of substrates are listed in **Table S4**. The relationship between the initial reaction rate and a substrate concentration (ranging from 1 to 1000 μM) were determined for each substrate in three independent experiments. The kinetic parameters K_M and V_{max} were calculated using Hans-Volf plot and ANOVA calculator.

Confirmation of the enzymatic activity. To verify if the observed quorum quenching activity is indeed coupled to the action of ecPGA, its activity was determined at increasing enzyme concentrations: 1.5, 3.0, 30 and 250 μM. The reaction was started by adding the enzyme into reaction mixture containing 10 mM of C06-HSL as a substrate at 0.05M phosphate buffer at pH 7 and temperature of 35°C.

RESULTS

Arrangement of the acyl-binding cavity and catalytic machinery in ecPGA and paPvdQ enable productive binding and stabilization of moderately long HSLs. The behavior of acyl-binding cavities and catalytic residues of paPvdQ and ecPGA enzymes in the absence of HSLs was analyzed in three 500 ns long MD simulations. First, we used CAVER 3 tool to explore the ability of these cavities to open their entrances wide enough to let the acyl-chain of substrate molecules in.[84] We observed frequent opening events in at least 10 % (ecPGA) and 20 % (paPvdQ) of each of three replicates (**Figure S6-S7**), providing ample opportunities for ligands to access these acyl-binding sites. Next, we investigated the overall geometric profiles of the acyl-binding cavities well-shaped for binding of the shortest ligand under consideration (C06-HSL) considering not only the entrance bottleneck but also the depth of the cavity and the appropriate location of the entry in the proximity to catalytic residues (**Table S5**). The examination of profiles of all open conformation of binding sites highlighted that the entrance to the cavity was broader and more than twice shorter in the case of ecPGA compared to paPvdQ (**Figure S8**). In both enzymes, the acyl-binding cavities adopted geometries that enabled binding of short-chain HSLs (**Table S5**). These geometries are consistent with the corresponding crystal structure geometries and imply that ecPGA facilitates sufficient opening and geometrical predisposition for binding of short-to-medium long acyl-chain HSLs and suggests the lack of the activity toward such compounds has to arise from another factor.

To further understand the difference between ecPGA and paPvdQ, we evaluated the dynamics of crucial functional atoms of catalytic residues. Importantly, the mechanism-based geometrical criteria defining arrangements of these atoms crucial for the activity of N-terminal serine hydrolases can be formalized as simultaneous fulfillment of the following requirements (**Figure 3**)–relatively short nucleophile attack distance (< 3.3 Å), two hydrogen bond stabilizations provided by the oxyanion hole stabilizing residues, and nucleophile attack angle ($\sim 90°$).[53,57,85]

In the light of these criteria, we considered the distances between N-terminal serine hydroxyl oxygen (Ser1β-O-hydroxyl) responsible for the nucleophile attack[86] and two nitrogen atoms of oxyanion hole stabilizing residues acting as hydrogen bond donors (Ala69β/Val70β-N-backbone and Asn241β/Asn269β-N$^\delta$, the identity of residues in ecPGA/paPvdQ, respectively),[70] the distance between these two oxyanion hole stabilizing hydrogen bond donors, and finally the distance between the Ser1β-O-hydroxyl and backbone oxygen of glutamine/histidine (Gln23β/His23β-O-backbone) known to additionally stabilize the ligand during the reaction.[48] PCA built on top of the network of these distances was used to map the

most relevant conformational transitions of the catalytic machinery (**Figure 4**). The first and second principal components (PC1 and PC2) used in the analysis cumulatively explained 78% and 84% of the total variance in these distances for ecPGA and paPvdQ, respectively. PC1 mainly reflected a change in the separation of Asn241β/Asn269β from Ser1β and Ala69β/Val70β, whereas changes along PC2 were mainly governed by the distance between Ser1β and Gln23β/His23β (**Table S9**).
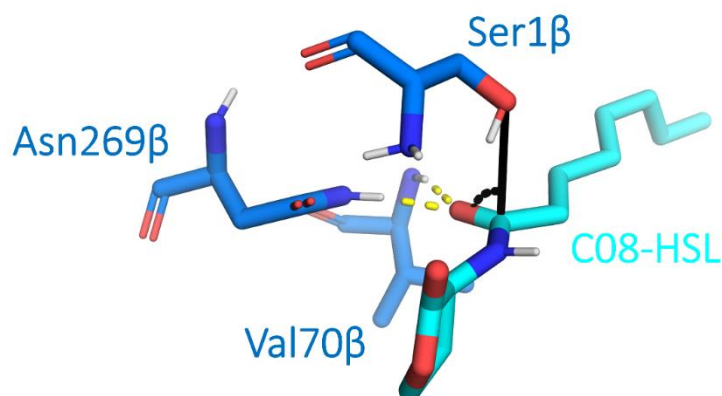

Figure 3. Interaction criteria required for productive stabilization of HSL illustrated on paPvdQ-C08-HSL complex. These criteria include nucleophile attack distance and angle (black lines), as well as two oxyanion hole stabilizing hydrogen bonds (yellow dashed lines).

Based on the highest density peaks in the conformational landscape formed by these two PCs, we elucidated the four most frequently visited **states a-d** (**Figure 4** and **Table S6**). Comparative analysis of both enzymes indicated that the four identified states correspond well to each other in terms of the arrangement of catalytic residues. Primarily, **state b** resembles favorable pre-organization of catalytic site for productive stabilization of HSLs in which nucleophile serine oxygen was within comparable distances to functional atoms of Ala69β/Val70β, Asn241β/Asn269β and Gln23β/His23β and hydrogen-bonded to backbone hydrogen of Gln23β/His23β (**Table S6**). Such arrangement enabled stabilization of HSL in the proper orientation for nucleophile attack reaction, i.e., having Ser1β hydroxyl oxygen approximately perpendicular to the plane of attacked amide bond of the ligand. On the other hand, the remaining three states would need to undergo conformational rearrangements to enable proper HSLs binding. In the **state a**, nucleophile serine hydroxyl group was in hydrogen bond distance to Ala69β/Val70β and Asn241β/Asn269β and more distant from the Gln23β/His23β (**Table S6**). In the case of this active-site conformation, the hydroxyl group of Ser1β blocked the access to oxyanion hole stabilizing residues, essentially preventing the binding of HSLs into reactive-like poses. Interestingly, **state a** was more common than **state b** in apo-form of ecPGA, while paPvdQ explored these states nearly equivalently, suggesting

paPvdQ to be better pre-organized for productive HSLs binding and stabilization. On the other hand, **state c** had nucleophile serine hydroxyl group in hydrogen bond distance to Ala69β/Val70β similar to **state a**, preventing potential oxyanion hole stabilization. More, the Asn241β/Asn269β occupied a flipped conformation (compared to **states a** and **b**) rendering its crucial nitrogen atom too distant from the remaining elements of the catalytic machinery for efficient HSL stabilization. The geometry of the **state d** resembled a combination of **state c** in terms of the Asn241β/Asn269β side-chain flip and **state b** for the geometry of remaining residues. **State d** would require conformational rearrangement of Asn241β/Asn269β residue for the favorable pre-organization for ligand stabilization. Importantly, **states c** and **d** were visited markedly less frequently compared to the remaining two states (**Table S6**), spawning **states a** and **b** as the most prominent out of the four analyzed.

Detailed investigation of the binding site dynamics combined with inspection of the behavior of catalytic residues enabled us to extract sufficiently open and appropriately pre-organized states of both ecPGA and paPvdQ enzymes for HSLs binding (**Table S5**). Next, we performed molecular docking of two moderately long HSLs: C06-HSL known to be cleaved by kcPGA[51] and C08-HSL as one of the shortest confirmed substrates of paPvdQ.[47,49] The docked poses underwent the abovementioned geometrical filtering based on the reaction mechanism to select complexes in configurations with properly stabilized ligand, which promoted the nucleophile attack reaction to occur. This procedure resulted in two to three well stabilized reactive binding poses per complex, with all distances within specified criteria and favorable binding energies estimated by Autodock4.2 scoring function (**Table S7**),[71] indicating that both enzymes exhibited favorable geometries of the acyl-binding cavities for accepting moderately long HSL and the arrangement of catalytic machineries was properly pre-organized for their productive stabilization.
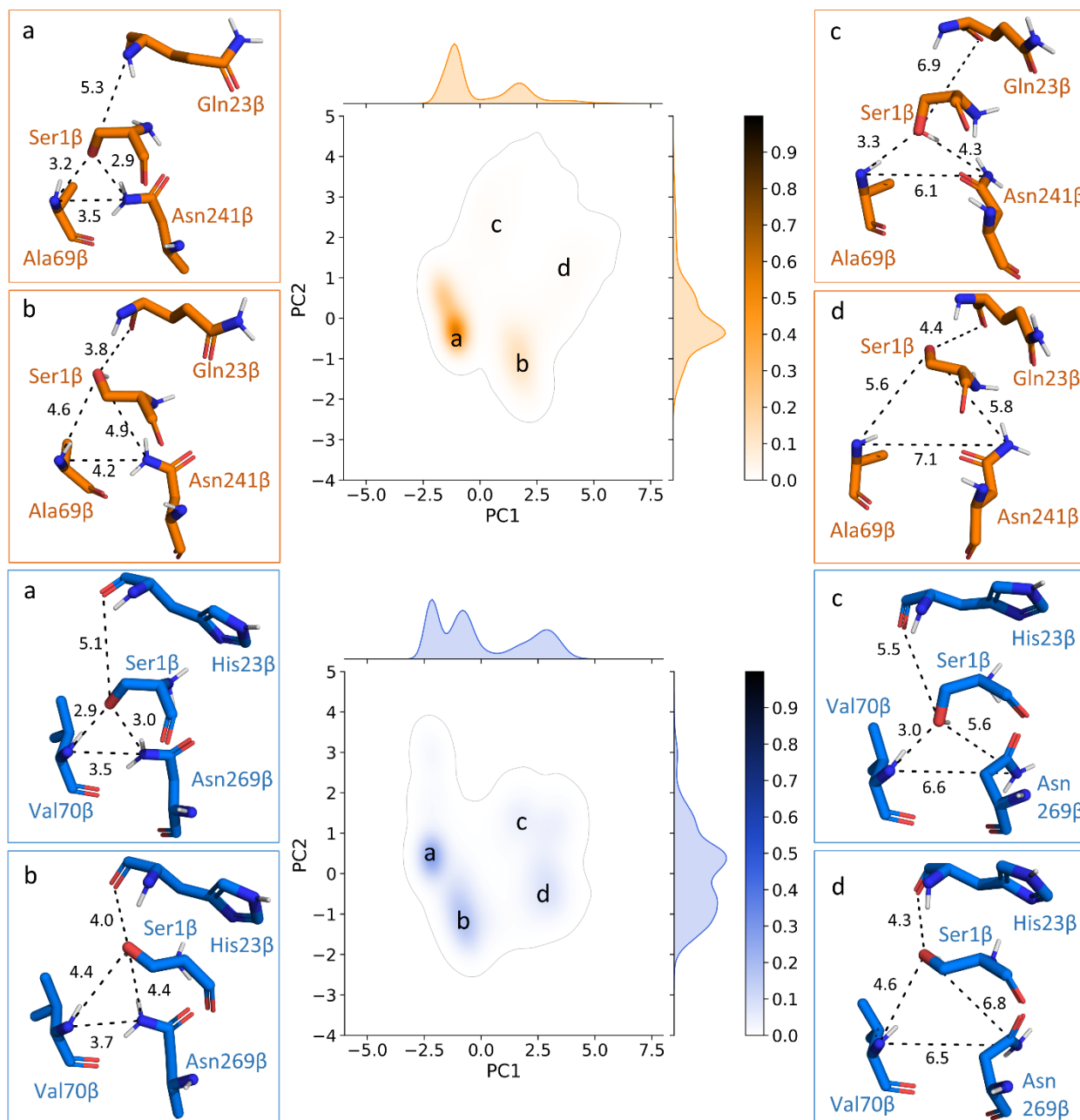
Figure 4. Primary conformations adopted by catalytic machinery of paPvdQ and ecPGA. PCA analysis of the ecPGA (top part, orange) and paPvdQ (bottom part, blue) based on catalytic residues distances obtained from MD simulations without substrates. States b represent catalytic residues favorably pre-organized for productive substrate binding. The remaining states (a, c, and d) require conformational re-arrangements to enable productive substrate binding.

Both enzymes maintain the productive stabilization of HSLs with a preference for paPvdQ over ecPGA. To compare the ability of both enzymes to maintain the productive binding of HSLs, we have performed 15 replicated simulations starting from their bound poses. On the grounds of the reaction mechanism utilized by N-terminal serine hydrolases,

14

analogously to Novikov *et al*.,[53] we have established criteria defining productive stabilization of the ligand in the acyl-binding site, which promote the initiation of the nucleophile attack reaction. These criteria were composed of the elements specified for the filtering after docking including: nucleophile attack distance, hydrogen bond stabilization provided by the oxyanion hole stabilizing residues, and were additionally extended by nucleophile attack angle expected to fall between 75° and 105°, to incorporate accessibility of the attacked carbonyl carbon of the substrate (**Figure 3**).

Initially, all stabilization components were evaluated simultaneously in two stages. First of all, we have searched for all states where nucleophile distance, angle and oxyanion hole was stabilized at once. Further, we quantitatively evaluated whether such fully stabilized states were maintained repetitively across the simulation or instead represented a random incident. We observed that paPvdQ maintained complete stabilization more frequently compared to ecPGA (**Figure S9-S10)**, although the latter was capable of attaining so as well. Notably, the difference between both proteins was emphasized more in the case of complexes with C08-HSL, for which we detected 3 replicas exhibiting repetitive formation of productive configurations for ecPGA and 11 replicas for paPvdQ. This trend is consistent with the preference for shorter substrates observed in the related kcPGA.[51] On the other hand, repetitive productive stabilization of C06-HSL was comparable between ecPGA and paPvdQ, detecting 9 and 13 such simulations, respectively. Interestingly, ecPGA provided very persistent stabilization of this shorter ligand in productive configurations that lasted almost the entire simulation in some of the simulations (**Figure S9**, replicas 8 and 14 of ecPGA-C06-HSL).

Further, we dissected the contribution of each of the features responsible for substrate stabilization. The nucleophile attack distance reached the required distance in simulations of both enzyme complexes with C06-HSL and C08-HSL. However, there was a clear preference towards paPvdQ for which the positioning of the ligand most frequently resulted in optimal attack distance (**Figure 5**). Similar observations concerned the nucleophile attack angle distribution (**Figure 5**). Here, the paPvdQ sustained the HSL properly oriented with carbonyl carbon exposed for the attack, while for ecPGA the distribution was significantly wider, having the attack angle more frequently in unfavorable regions. Analogous investigation of the distances responsible for stabilization of the oxyanion hole showed that these interactions were also properly kept in both proteins (**Figure S11**). Interestingly, paPvdQ complexes featured a larger asparagine distance, which was coherent with observations from PCA of free-enzyme simulations showing that **states c** and **d** (**Figure 4**) with the flipped asparagine conformation were more prevalent in paPvdQ compared to ecPGA.
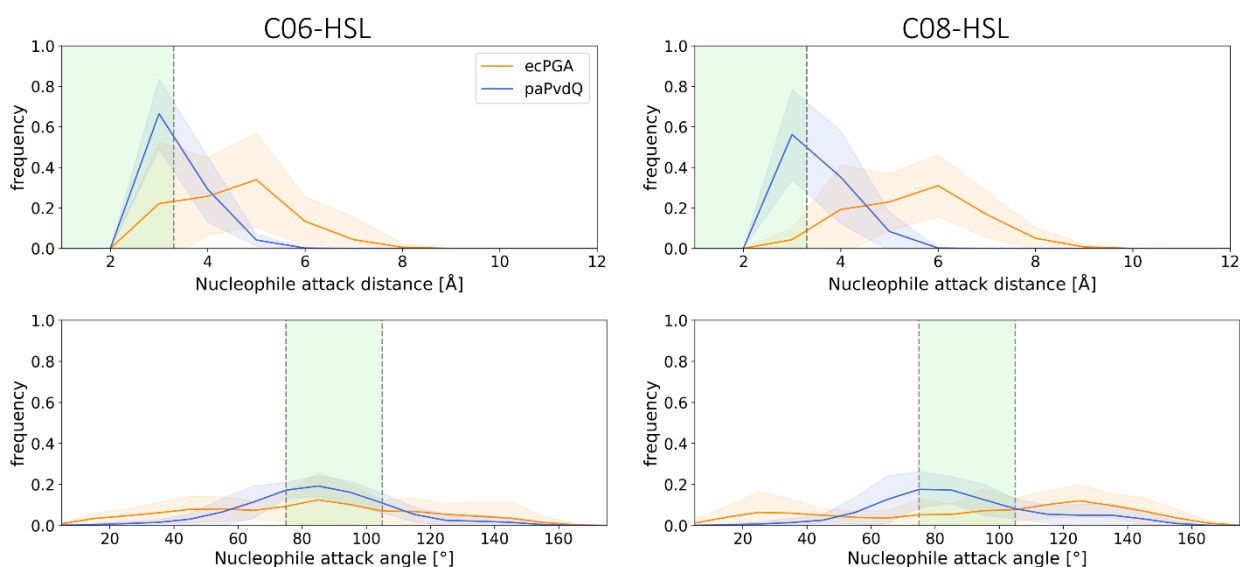
Figure 5. Maintenance of the properly stabilized protein-ligand complexes. Distribution of nucleophile attack distance (upper plots) and angle (bottom plots) for ecPGA (orange) and paPvdQ (blue) enzymes in complex with C06-HSL (left) and C08-HSL (right) from simulations where the average ligand RMSD did not exceed 5.0 Å (Figure S12-13). Regions of the plots highlighted in green indicate the optimal range of the parameter.

To further understand factors that contributed to the apparent difference in substrate stabilization, we explored the mobility of individual heavy atoms of HSL (**Figure 6**). Conducted analysis consistently indicated that the most mobile part of the ligand in all complexes was represented by the exposed lactone ring, followed by atoms of scissile amide bond stabilized by interactions with residues of catalytic machinery, and lastly, the acyl-chain buried in the binding site. For the complexes of the C06-HSL, the fluctuations of atoms were comparable between the two enzymes, although they exhibited slightly higher values of standard deviation for ecPGA than for paPvdQ. A more pronounced difference was observed for the longer substrate, where although the overall trend of the fluctuations was similar for both systems, the absolute fluctuations were higher in the case of ecPGA. This correlated well with the acyl-binding cavity profiles (**Figure S8**), showing that the entry to the acyl-binding pocket of ecPGA was wider and more shallow, hence providing more conformational freedom to ligand molecule which in turn resulted in less optimal stabilization, especially for the longer substrate that could not be fully accommodated inside the pocket.
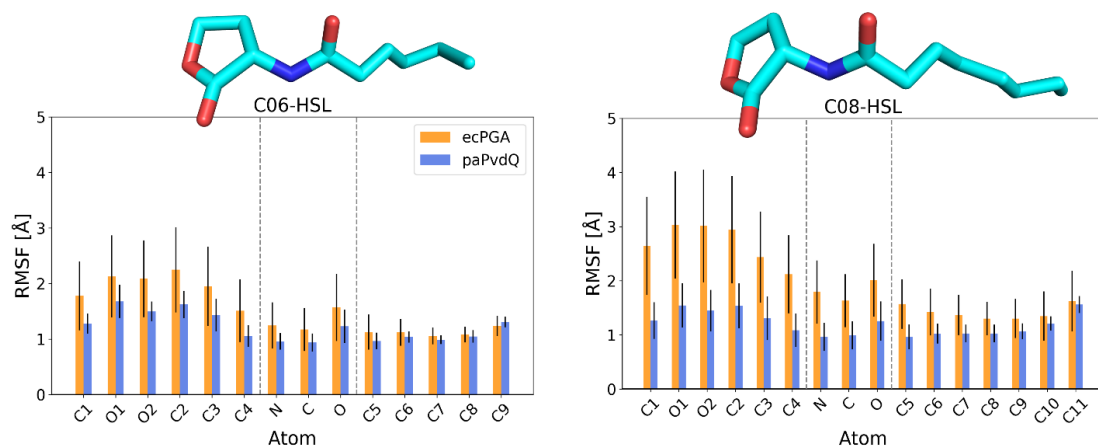
16

Figure 6. The mobility of the HSL atoms during simulations. Root-mean-square fluctuation (RMSF) of HSL heavy atoms in simulations where the average ligand RMSD did not exceed 5.0 Å (Figure S12-13).

Finally, we estimated the binding free energies of productively bound protein-ligand complexes using the MMGB/SA method. The obtained binding energies were favorable for both ligands in both paPvdQ and ecPGA and proportional to the size of the ligand (**Table S8**). A per residue decomposition of these binding free energies elucidated the main difference for residues Met142α, Phe146α, and Phe256β in ecPGA which correspond to regions in which the backbone of these two proteins cannot be spatially aligned (**Figure S14**). Met142α forms the bottom part of the cavity for ecPGA, which in the case of paPvdQ is significantly more buried in the protein core, while Phe146α contours the entrance to the acyl-binding cavity being wider in ecPGA (**Figure S8**). Phe256β in ecPGA interacted with the lactone ring of the ligand from the outside of the cavity which was distinct only for this protein in complex with C06-HSL. These residues, although contributing favorably in the case of short to medium-length ligands, can potentially play a central role in preventing efficient binding for longer substrates, as observed for kcPGA.[51] On the other hand, for paPvdQ residues Phe32β and Trp186β (**Figure S14**), which are located approximately in the middle of the acyl-binding cavity (corresponding to the bottom part of the cavity in ecPGA), contributed favorably as they narrow this part of the cavity to stabilize the alkyl chain of the substrate and restrict its mobility. The remaining residues did not differ significantly in their contributions to the binding free energy.

Initiating N-terminal serine hydrolases acylation. Encouraged by computational predictions indicating that ecPGA was able to productively bind and stabilize HSLs motivated us to further investigate their putative degradation mechanism. Here we focused on the acylation that is assumed to be the rate-limiting step for hydrolysis of similar classes of substrates by acylases and serine proteases.[87–89] First, we scrupulously selected protein-ligand complexes with the configurations most favoring the reaction from the previous simulations

17

(**Table S10**) and performed restrained simulations to generate a uniform ensemble of Michaelis complexes (MCs) as starting positions for replicated steered QM/MM MD simulations (**Figure S15**). Next, we executed QM/MM MD simulations mimicking the mechanism defined by Grigorenko *et al*. for ecPGA with its native substrate–penicillin G,[69] i.e., we simulated the acylation in two steps including (i) nucleophilic attack by Ser1β that is directly activated by its own α-amino group leading to the formation of TI, followed by (ii) the decomposition of TI into the AE complex and release of the first reaction product–homoserine lactone (**Table S11**).

Nucleophile attack is concerted with proton transfer from serine hydroxyl to its amine group and is feasible in both enzymes. Starting from the MCs (**Figure 7** and **Table S12**), we performed simulations of the proton transfer between hydroxyl oxygen and amine nitrogen of nucleophile Ser1β (**Figure 2A**). During the transfer process, we observed a spontaneous nucleophile attack that resulted in up to 0.5 Å shorter distance between nucleophilic oxygen and the attacked carbon of the HSL in MC (RC 1.1 Å) and TS1 (RC ~ 0.2 Å) states (**Table S12**). Such a concerted mechanism is in the agreement with the mechanisms of conversion of penicillin G by ecPGA.[69] Interestingly, the observed shortening of the distance was prominent while the proton was located approximately equidistantly between these two groups (RC ~ 0.0 Å) for all systems except ecPGA-C08-HSL, in which the formation of TS1 and subsequent creation of a covalent bond between the substrate and Ser1β were notably delayed to RC 0.1 Å and RC -0.2 Å, respectively (**Figure 7** and **Figure S16**). The whole step was completed once the proton was fully transferred to the amine nitrogen of Ser1β and a stable TI was formed (**Table S12**). Visual inspection of the TI structure revealed the following structural hallmarks (**Table S12**): formation of the covalent bond between nucleophile oxygen and attacked carbon of the substrate at 1.5-1.6 Å, stabilization by enhanced hydrogen bonding with residues Ala69β/Val70β (1.9-2.0 Å), Asn241β/Asn269β (1.9 Å) and Gln23β/His23β residue (2.1-2.3 Å), elongation of the scissile bond between amide nitrogen and attacked carbon of the substrate by 0.1 Å (from 1.4 to 1.5 Å), and reduction of the distance between one of the amine group hydrogens of Ser1β to the amide nitrogen of the substrate, hence promoting its readiness for a second proton transfer in the subsequent step. The activation barrier connected with TS1 was ca. 7 kcal/mol except for ecPGA-C08-HSL in which reaching TS1 was energetically more demanding by >1.2 kcal/mol compared to the other investigated systems (**Table S13**). Structurally, this higher barrier in ecPGA-C08-HSL was characterized by increased nucleophile attack distance (2.7 ± 0.4 Å) and its preference to interact with the oxyanion hole stabilizing residue Asn241β over Ala69β (**Table S12**).
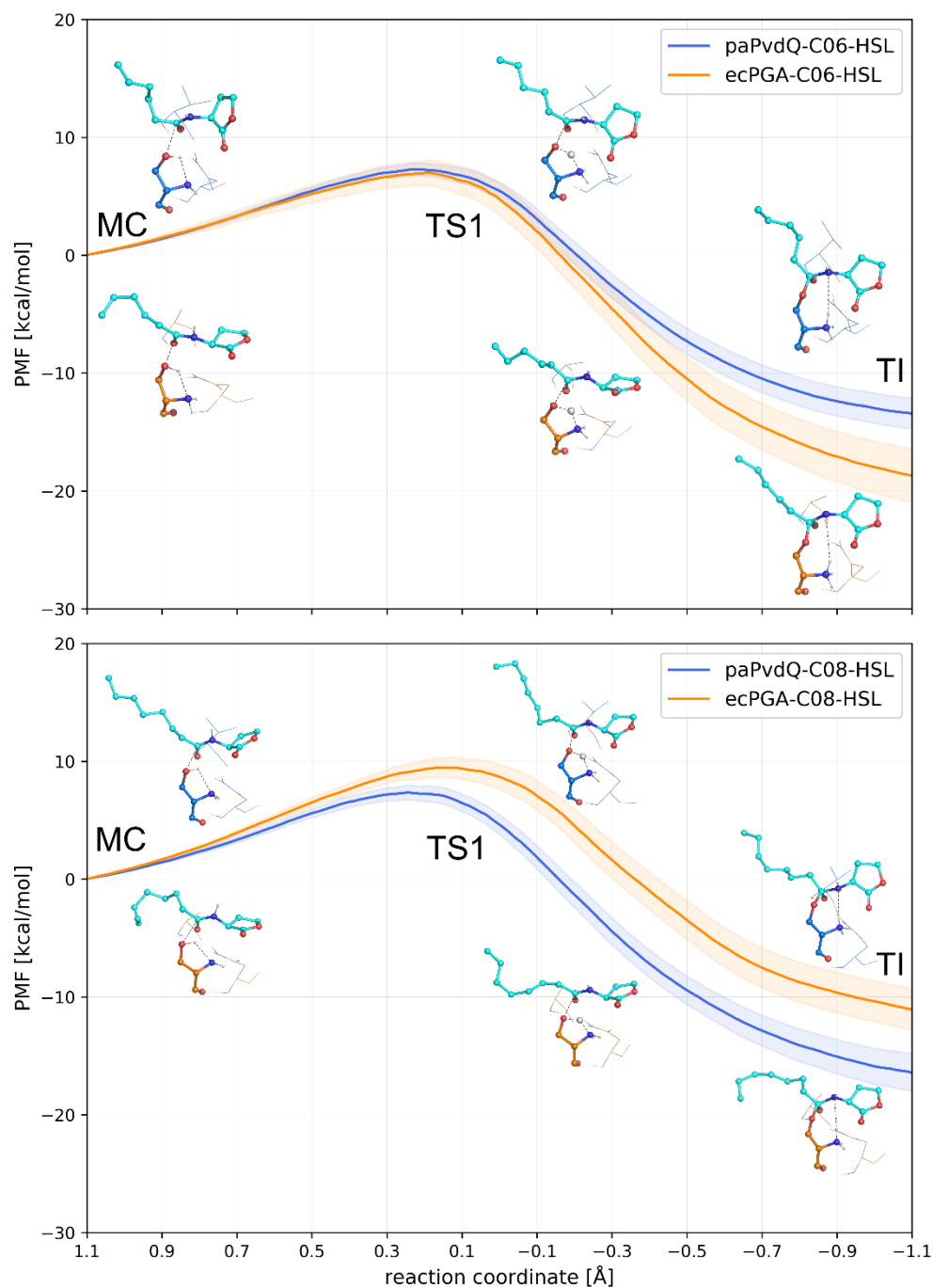
Figure 7. Potential of mean force profiles from steered MD simulations of the tetrahedral intermediate formation step. C06-HSL (upper panel) and C08-HSL (lower panel) acylation catalyzed by ecPGA (orange) and paPvdQ (blue) enzymes. Starting from the MC (RC 1.1 Å), systems proceed towards TS1 (RC ~ 0.2 Å) where the catalytic serine hydroxyl hydrogen was shared between its hydroxyl and amine group, which was synchronized with the nucleophile attack of the hydroxyl oxygen to the substrate carbonyl carbon and resulted in TI formation (RC -1.1 Å).

In both enzymes, proton transfer initiates the amide bond cleavage leading to acyl-enzyme formation. Continuing from the ensembles of TI states for each protein-HSL complex, we simulated the second step of the acylation process, i.e., the decomposition of TIs to respective AEs (**Figure 8**, **Table S12**). During this process, the proton transfer between amine nitrogen of Ser1β and the amide nitrogen of the leaving group preceded the cleavage of the amide bond, each stage exhibiting separate energy maxima TS2a and TS2b (**Figure 8 and Table S14**). The first maximum TS2a corresponded to the scenario in which the transferred proton was shared between serine amine nitrogen and the amide nitrogen of the leaving group but already closer to the latter (RC ~ 1.9 Å), which was accompanied by a mild extension of the scissile bond from 1.5 Å in TI to 1.6 Å in TS2a (**Figure S17** and **Table S12**). The elongation of the scissile amide bond became much more pronounced after the proton was fully transferred to the substrate nitrogen (RC ~ 3.0 Å); proceeding towards a fully broken bond at the distances ≥3.3 Å (**Figure S17** and **Table S12**). The second energy barrier connected with the bond cleavage process (TS2b) coincided with the length of the amide bond of 1.8-2.0 Å (RC ~ 3.3 Å). The energy maximum connected with the bond breaking (TS2b) was lower by up to 0.5 kcal/mol compared to the one coupled mainly with the proton transfer (TS2a) in the case of both ecPGA complexes (**Table S14**). In contrast, the breaking of the amide bond (TS2b) was more demanding by 0.8-1.6 kcal/mol for both HSLs in the case of paPvdQ (**Table S14**).
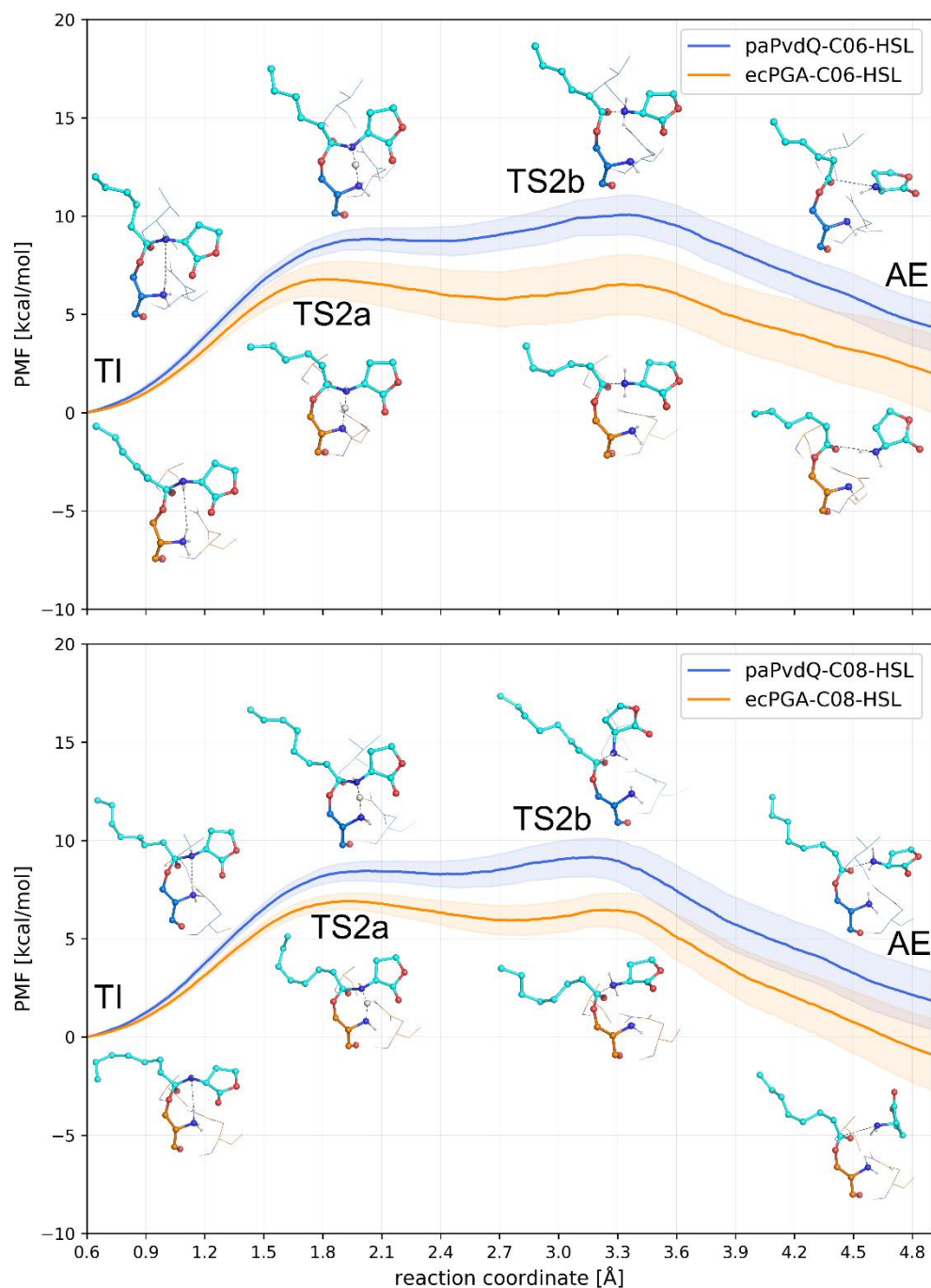
Figure 8. Potential of mean force profiles from steered MD simulations of the acyl-enzyme formation step. C06-HSL (upper panel) and C08-HSL (lower panel) acylation performed by ecPGA (orange) and paPvdQ (blue) enzymes. Starting from the TI (RC 0.6 Å), systems follow towards TS2a (RC ~ 1.9 Å), corresponding to the proton shared between the catalytic serine amine group and the nitrogen of the leaving group. Further, the proton was fully transferred to the leaving group nitrogen and the amide bond was broken, accounting for TS2b (RC ~ 3.3 Å). Finally, the first reaction product, homoserine lactone, was released from the active site and resulted in AE formation (RC 4.9 Å).

Experimental assays confirm the computational prediction of ecPGA QQ activity.
Driven by encouraging computational predictions we have experimentally evaluated the activity of ecPGA towards C06- and C08-HSLs. First, we examined spontaneous hydrolysis of C06-HSLs in abiotic conditions for different substrate concentrations (5, 10, and 20 mM) at pH 7.0 and temperature 35°C, optimal for ecPGA. Further, these assays were compared with samples of C06-HSL substrate at different increasing concentrations of ecPGA in the range of 1.5-250 µM. The samples containing ecPGA indicate by far more efficient hydrolysis of C06-HSL compared to uncatalyzed ones (**Figure 9**). Additionally, we detected proportionally higher amounts of the hydrolyzed substrate with increasing concentration of the enzyme, clearly demonstrating the ability of ecPGA to catalyze HSLs hydrolysis.

Having the ecPGA activity towards HSLs confirmed, we determined the kinetic parameters of this enzyme with both investigated substrates (**Figure S18**). For C06-HSL, the K_M and k_{cat} kinetic constants were 0.59 ± 0.07 mM and 0.0090 ± 0.0003 s^{-1}, respectively. Whereas for the longer substrate, C08-HSL, the obtained parameters were less favorable, reaching K_M of 0.70 ± 0.04 mM, and k_{cat} of 0.0085 ± 0.0003 s^{-1}. The determined kinetic constants were in agreement with our computationally estimated preference for shorter substrates conditioned by less favorable stabilization of the substrate in productive conformation and higher undesirable fluctuation of the lactone ring and cleaved amide bond.
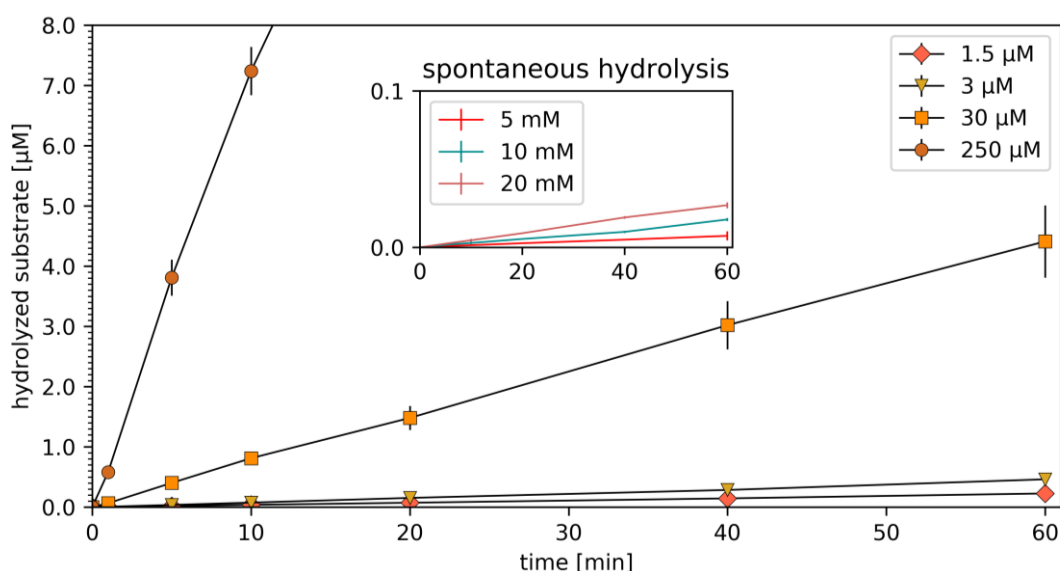

Figure 9. Experimental examination of ecPGA catalytic activity. Dependence of the enzyme concentration on the hydrolyzed substrate concentration (main plot) indicated increasing concentration of the hydrolyzed substrate with increasing enzyme concentration. The inset plot represents spontaneous substrate hydrolysis under the same reaction conditions but without addition of ecPGA enzyme.

Computational and experimental analyses confirm the HSL-degrading activity of remotely related aPGA. Confirming that indeed the ecPGA is active against two tested HSLs, we decided to probe QQ activity also for a more distant member of the PGA family to see how widespread it is among Ntn-hydrolases. For this purpose, we selected aPGA which is well established in our laboratory and importantly, it is only ca. 60 % similar to both kcPGA and ecPGA (**Table S1**), and also carries Val56βLeu substitution located directly in its active site.

Based on the free enzyme MD simulations, efficient sampling of the open acyl-binding cavity was observed with a frequency >6% (**Figure S22**), indicating that aPGA was also capable of adopting conformational states spatially sufficient to accept HSL with short or moderately long acyl chain (**Table S15**) and interestingly exhibited wider entrance to the acyl-binding cavity compared to ecPGA or paPvdQ enzymes in all three simulations (**Figures S8 and S23**). PC1 and PC2 derived from PCA built based on the distances between functional atoms of catalytic residues explained 75% of their total variance. In contrast to the outcomes of PCA of other two proteins, PC1 mainly correlated with the distance between Ser1β and Gln23β/His23β, whereas changes along PC2 followed the distance between Asn241β/Asn269β and Ala69β/Val70β (**Table S18**), forming an almost inversed picture of the conformational landscape (**Figure S24**). All four most prevalent conformational states resembled **states a** and **b** observed in ecPGA and paPvdQ (**Figure S24, Table S16**). In **states a** and **a***, the serine hydroxyl oxygen was more distant from Gln23β and hydrogen-bonded to oxyanion hole stabilizing residues disallowing the reactive binding of HSLs. **States b** and **b*** stabilized by hydrogen bonding with backbone hydrogen of Gln23β corresponded to the favorable organization of the catalytic site for productive stabilization of HSLs, although the distance between oxyanion hole stabilizing residues was higher than in the case of ecPGA and paPvdQ, which was conditioned by the more pronounced opening of the entrance to the acyl-binding site observed for this enzyme. Consequently, the selection of appropriately pre-organized open snapshots resulted in a smaller ensemble of snapshots for docking (**Table S15**). Nevertheless, molecular docking provided aPGA in complex with C06-HSL and C08-HSL substrates properly stabilized to promote nucleophile attack reaction, without compromising geometry-based selection criteria or favorable binding score (**Table S17**).

Analogously to the remaining two proteins under investigation, MD simulations of aPGA-HSL complexes were explored to determine the ability of this enzyme to maintain the crucial interactions of the ligand with catalytically relevant residues. As expected, aPGA presented similar behavior to ecPGA, which means that the evaluated distances and angle reached optimum values across the simulations, although notably less frequently than in paPvdQ

23

(**Figure S25**). Additionally, repetitive stabilization of the ligand in a productive state, shown in **Figure S26,** was more frequently observed for C06-HSL (5 replicas), compared to C08-HSL (2 replicas), highlighting the binding preference of aPGA towards shorter ligand, consistently to ecPGA. However, we also noted increased instability of HSLs bound in aPGA, often observing even total dissociation from the active site (**Figure S27**) compared to highly stable complexes formed with ecPGA (**Figures S12 and S13**). Mobility of the HSL heavy atoms indicated that in the case of aPGA, the most mobile part of the ligand was also the lactone ring, followed by the atoms of the amide bond and the acyl-chain (**Figure S28**). The amplitudes of fluctuations of C08-HSL were similar to those observed in ecPGA, however, most of the atoms of C06-HSL exhibited significantly larger fluctuations in aPGA, enabled by the wider opening of the acyl-binding cavity in this enzyme. Finally, binding free energy elucidated that aPGA bound HSLs as tightly as ecPGA, either in terms of the absolute energy (**Table S19**) or the particular contributions from each residue (**Figure S29**).

Progressing towards examining acylation reaction by steered QM/MM MD simulations, we had to relax the selection criteria for structures from aPGA-C08-HSL due to lack of optimally stabilized representatives sampled in the simulations (**Table S20**). Nonetheless, the selected structures were sufficiently close to the desired parameters to still enable their adjustment during restraint MD simulations and the following generation of an appropriate ensemble of MCs as starting positions for QM/MM MD simulations (**Table S21**).

Reaction mechanisms observed for aPGA with C06-HSL and C08-HSL during TI and AE formation steps proceeded through TS1, TS2a, and TS2b in a manner consistent with the mechanisms observed for ecPGA and paPvdQ enzymes (**Table S22** and **Figures S30-S33**). Curiously, the energy barrier at TS1 for aPGA-C06-HSL (**Table S23**) was similar to ecPGA-C08-HSL and notably higher than remaining complexes at this reaction step (**Table S13** and **S23**). Analogously to ecPGA-C08-HSL, we observed delayed nucleophile attack by Ser1β also for aPGA-C06-HSL (**Figure S32**), yielding increased nucleophile attack distance in TS1. However, in the case of this substrate, its carbonyl oxygen was closer to Ala69β rather than to Asn241β (**Table S22**).

Surprisingly, the energy barrier for the second step of the reaction for aPGA enzyme with C08-HSL reached a higher value of 9.0 ± 0.7 kcal/mol in TS2a (**Table S24**), which was much larger than observed for ecPGA and comparable to the energy levels for paPvdQ in this state (**Table S14**). Nonetheless, the overall energy cost of traversing along the RCs in aPGA was comparable to the other two investigated systems, with TS2a and TS2b located at similar points along the RC, suggesting that also aPGA has the ability to hydrolyze C06- and C08-HSLs.

To validate those findings, we determined the kinetic parameters of aPGA with both substrates. The observed K_M values of 0.62 ± 0.1 mM (C06-HSL) and 0.87 ± 0.01 mM (C08-HSL) were higher than the respective values for ecPGA, which corresponded well with the computational observation of less frequent productive stabilization of substrates by aPGA compared to ecPGA. aPGA exhibited catalytic rates of 0.0079 ± 0.0003 s^{-1} and 0.0064 ± 0.0001 s^{-1} for C06- and C08-HSLs, respectively (**Figure S19**).

Dynamic determinants of quorum quenching activity in N-terminal hydrolases. Intensive computational study and experimental validation concurred that all three studied representatives of the N-terminal serine hydrolase family–aPGA, ecPGA, and paPvdQ–possess appreciable activity towards C06- and C08-HSLs. Importantly, we observed system-dependent conformational and energetic preferences governed by several dynamic determinants primarily connected with the behavior of the two molecular gates, (i) gates to the acyl-binding cavity, and (ii) gates controlling overall accessibility of the active site.

At the first acylation step, aPGA-C06-HSL and ecPGA-C08-HSL complexes presented increased energy barriers compared to the remaining systems. In both cases, the reason for the energy barrier rise was accompanied by suboptimal oxyanion hole stabilization, although with a different shift from the optimum. As illustrated in **Figure 10A**, in aPGA C06-HSL tended to interact stronger with Ala69β, which more frequently sampled slightly different side-chain conformation compared to other systems corresponding to **state b*** identified in PCA analysis (**Figure S24**). This residue is located close to the acyl-binding site entrance which exhibited a more pronounced opening (**Figure S23**) coupled with frequent evasion from optimal interactions with Asn241β. On the other hand, ecPGA-C08-HSL exhibited opposite behavior resulting in oxyanion hole stabilization shifted more towards Asn241β (**Figure 10B**), which is located closer to the bulk solvent. In both cases, the deviation from the optimal oxyanion hole stabilization resulted in substrate molecule being located further from the nucleophile in both MC and TS1 (**Table S12 and S22**), causing the delayed formation of covalent bond (**Figures S16 and S32**) and less favorable energy barriers (**Figures 7 and S30**). In the remaining systems (**Figure 10C-D**), the TS1 stabilization was balanced in contributions from both oxyanion hole stabilizing residues, promoting closer distance of the nucleophile attack and lower energy barrier.
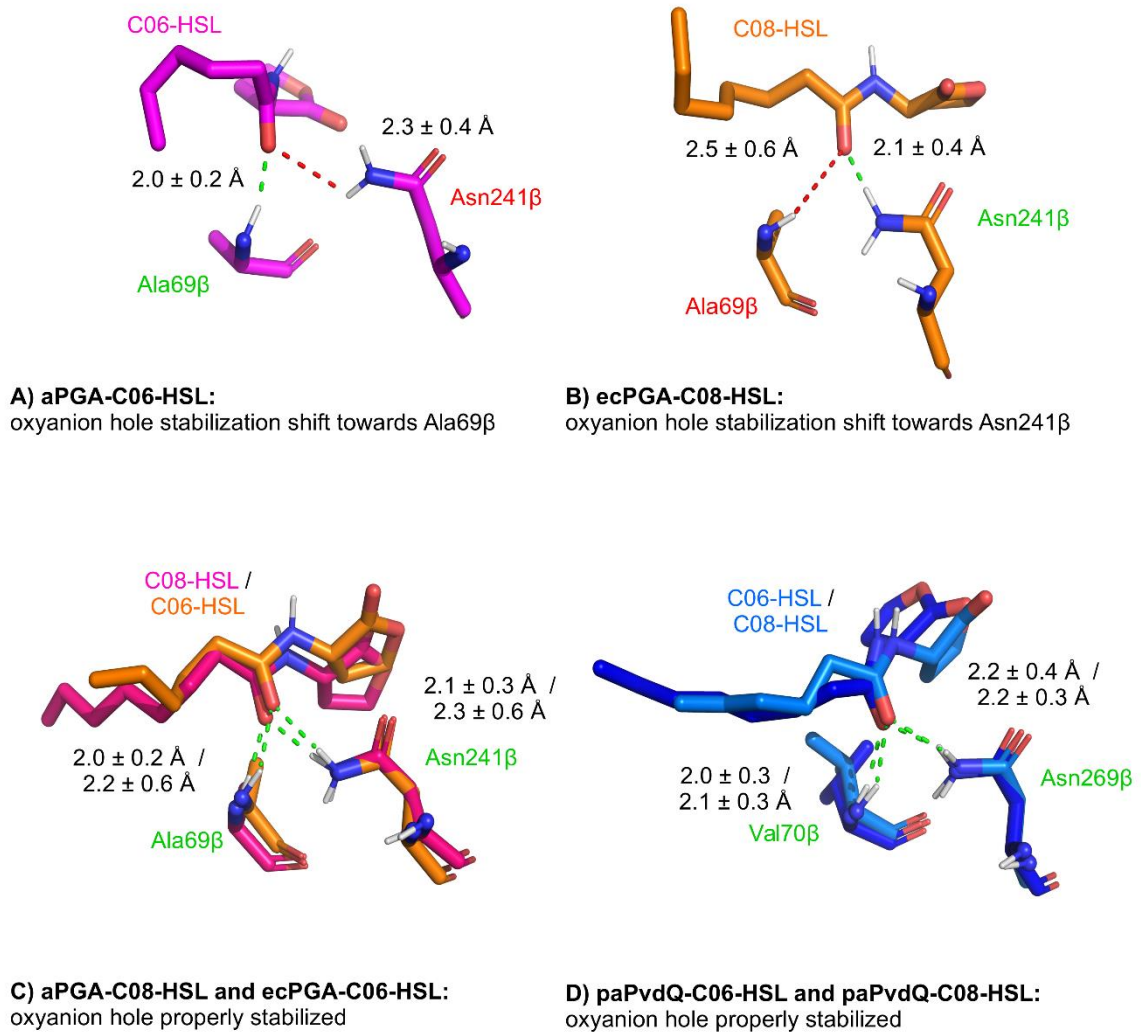
Figure 10. The difference in oxyanion hole stabilization in TS1 contributing to increased energy barriers for aPGA-C06 and ecPGA-C08 complexes. A) aPGA-C06-HSL complex with the shift of the HSL carbonyl oxygen towards Ala69β residue, B) ecPGA-C08-HSL complex with the HSL carbonyl oxygen preferentially stabilized by Asn241β. C) represents complexes of PGAs with properly stabilized oxyanion holes and D) analogous observation for both paPvdQ complexes.

To understand the difference between aPGA and ecPGA enzymes' preference, we focused on the sequential differences of the residues in the vicinity of the catalytic machinery and binding cavity, as the catalytic machinery is fully composed of the same amino acids. There are two differences in this region: (i) aPGA carries more bulky leucine in position 56β compared to valine in ecPGA, and (ii) ecPGA contains tyrosine in position 27β in contrast to tryptophan in aPGA. The residue at position 56β partially contributes to the depth of the acyl-binding cavity, making it slightly longer in ecPGA. The variability at position 27β results in distinct dynamics of gating residue Phe24β, the backbone of which is stabilized by hydrogen

bonding with the hydroxyl group of tyrosine side-chain in ecPGA or free to move in aPGA missing steric hindrance presented by the hydroxyl group (**Figure S34 and S35**). The increased mobility of the gate in aPGA is in conformity with the more pronounced opening of its acyl-binding site (**Figure S23**). Curiously, the availability of additional space resulted in favorable energetics for longer substrate but caused an undesired effect for C06-HSL which was bound too deep in the cavity and stabilized by the altered conformation of Ala69β (**Figure 10A**). Such opening of the acyl-binding site was not possible in the ecPGA enzyme because of the efficient stabilization of Phe24β by Tyr27β (**Figure S35**), which was favorable for a shorter substrate but less suited for C08-HSL which lacked the space to accommodate the long acyl-chain adequately. On the other hand, paPvdQ in complex with both ligands elucidated relatively steady behavior of the differently composed gate, resulting in a stable deep acyl-binding cavity (**Figure S36**). Furthermore, while inspecting the geometries of the HSLs in TS1 we observed a clear tendency of the HSL being more bent in aPGA to fit the broader cavity than the remaining two enzymes (**Figure S37A**).

As mentioned in the previous sections, energy barriers also varied for the second reaction step. This variation could be traced to differences in a relative arrangement of the Arg263β in PGAs and Arg297β in paPvdQ with respect to the amine group of Ser1β and leaving homoserine lactone oxygen (**Figure 11, Table S12** and **S22**). This arginine residue is known to play a crucial role in the acylation step catalyzed by the ecPGA enzyme and it is believed to be important for the catalytic activity of paPvdQ as well.[48,69,90] In paPvdQ, Arg297β was closer to the serine amine group and almost aligned with the direction of proton transfer, rendering the lactone oxygen of the substrate inaccessible. On the other hand, in PGAs Arg263β adopted different conformation further from the Ser1β amine group due to cation-pi interaction with Trp240β, which is missing in paPvdQ (**Figure 11**). This rearrangement promoted access of Arg263β to the lactone oxygen of HSL, enabling additional stabilization of the leaving group.
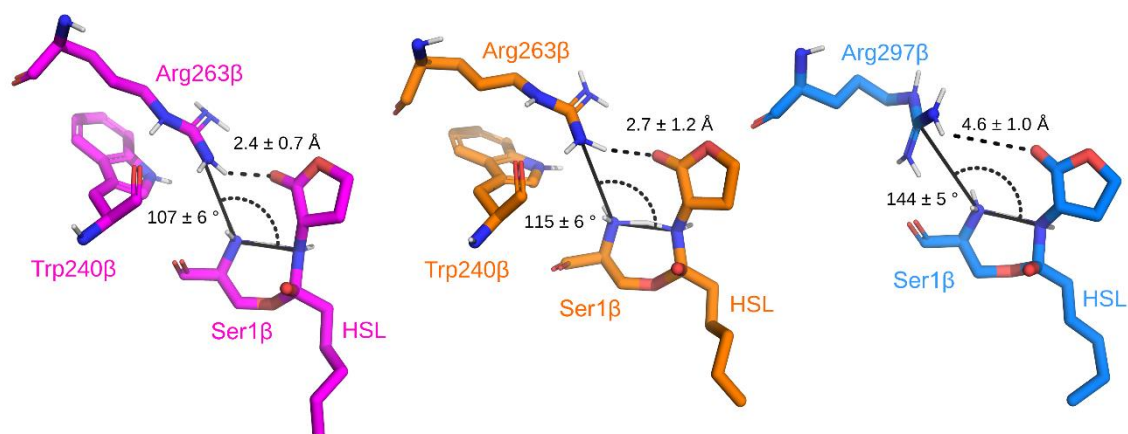
27

Figure 11. Different stabilization of TS2a by Arg263β in PGAs and Arg297β in paPvdQ. The arginine was, on average, closer to the Ser1β amine group and further from the lactone oxygen of HSL in paPvdQ (in blue). In contrast, the opposite situation was noticed in aPGA (in magenta) and ecPGA (in orange). The angle between HSL nitrogen, serine amine nitrogen and arginine guanidyl carbon was higher for paPvdQ blocking the access of arginine to the lactone of HSL. Also, note that the planes formed by guanidyl groups were approximately perpendicular between PGAs and paPvdQ.

Additionally, we observed higher energy barriers connected with both TS2a and TS2b for aPGA-C08-HSL compared to remaining PGAs' complexes. Interestingly, this complex had a higher tendency to sample the closed conformational state of the whole active site characterized by interactions between Arg145α and Phe24β (state **C** in **Figure S38**).[53,91] In this closed state, Arg145α is located in the proximity of the scissile amide bond in the substrate (ca. 7.5 Å) hereby interfering with the proton transfer. In aPGA, the formation of a closed state was facilitated by the Trp27β leaving the backbone oxygen of Phe24β more exposed to interactions with the guanidine group of Arg145α. Furthermore, the bent acyl-chain of C08-HSL (**Figure S37B**), which is not that prevalent in other investigated systems at this reaction stage, interacted preferentially with Phe146α leaving space for Phe24β to adopt the inclined conformation susceptible to Arg145α (semi-closed **C/O** and closed **C** states in **Figure S38**), hence promoting the formation of the closed state by aPGA. In ecPGA, the backbone oxygen of Phe24β was hydrogen-bonded with the hydroxyl group of Tyr27β effectively blocking its interactions with Arg145α and the adoption of the closed state (**Figure S39**). This agrees with the observation of Alkema and Novikov who showed the role of Arg145α residue in substrate specificity.[53,90]

DISCUSSION

Investigation of the QQ enzymes undoubtedly gained momentum in the recent decade. Plenty of new enzymes were shown to exhibit activity against various QS signaling molecules, hence expanding our knowledge and moving us closer towards QQ-based antibacterial strategies addressing problems of widespread antibiotic resistance and biofouling. Although the range of QQ enzymes known is already broad as comprehensively summarized in several recent reviews,[47,92] there are still crucial challenges that remain unsolved. Most of the characterized enzymes with high QQ activities have not been optimized for large-scale utilization. In contrast, enzymes, which are well-established and robust industrial catalysts, often exhibit only relatively low catalytic rates, complete lack of activity or problematic substrate specificities. This situation highlights the need for further work on elucidating the molecular determinants conditioning efficient QQ activity that would enable their effective transplantation into biotechnologically optimized enzymes.

Regarding N-terminal serine hydrolases, representing the main subject of this study, only a few reports aiming to understand their mode of action at the molecular level were presented up to date. In the case of paPvdQ, mechanisms of the catalytic action of this enzyme were initially hypothesized based on the crystallographic data for apo-enzyme,[48] and further extended by work on transition state analogoues[56] and mutations shifting substrate specificity towards C08-HSL.[49] Our study confirms that paPvdQ exhibited a deep acyl-binding pocket, which remained stable within the timescale of our simulations, contrary to PGAs with significantly shallower pockets. We verified the crucial importance of residues forming catalytic machinery besides Ser1β, including oxyanion whole residues Val70β and Asn269β, as well as additionally stabilizing His23β, as shown in previous studies.[48,49] Presented results demonstrated, that catalytic Ser1β is capable of self-activation through accepting hydroxyl oxygen by its N-terminal amine group without incorporating bridging water molecule, which is in agreement with observations made by Clevenger *et al.* for paPvdQ with transition state analogs and computations performed by Grigorenko *et al.* for ecPGA with penicillin G,[56,69] suggesting that such activation might indeed be a general property of N-terminal serine hydrolases and invariant to the substrate molecule involved. Our investigation accounting for the dynamical nature of biomolecular systems indicated that highly conserved Arg297β[48,56] tended to adopt different conformation compared to analogous Arg263β in PGAs, which contributes to increased energy barriers at the second step of the reaction for paPvdQ. Substrate specificity of paPvdQ towards four different QS signaling molecules C12-HSL, 3-oxo-C12-HSL,

C08-HSL and C04-HSL was also investigated by MD simulations that were often started from binding poses of substrate molecules rather distant from the catalytic residues.[93] As a consequence, these simulations have only infrequently or not at all explored catalytically competent states of paPvdQ within the employed timeframe of 300 ns as illustrated by the absence of productive binding modes in C08-HSL-paPvdQ complexes. When using the productive binding poses to initiate the simulations, we observed substantial capability of paPvdQ to stabilize and catalyze the conversion of not only C08-HSL but also C06-HSL, both expected to be productively bound and converted by this enzyme.[49,56,94] Based on these complexes, we could investigate molecular details of the catalytic action of this enzyme.

On the other hand, currently the only report regarding confirmed QQ activity among PGAs was presented by Mukherji *et al.* who experimentally verified QQ ability for kcPGA and defined the preference of the former enzyme for 3-oxo-C06-HSL.[51] Otherwise, the structure-dynamics-function relationships were mainly studied on the ecPGA with its native substrates or related compounds, due to the importance of this enzyme for the production of semi-synthetic antibiotics, employing experimental techniques and a broad spectrum of molecular modeling methods including docking, MD simulations, QM or QM/MM calculations.[53,57,69,70,85,95] In this view, our study provides a complementary extension of the current knowledge about N-terminal serine hydrolases towards their QQ action elucidated by the extensive QM/MM MD simulations, which to our knowledge were so far reported only for cysteine N-terminal-hydrolases—a closely related system that, however, behave differently from serine or threonine hydrolases due to preferable zwitterionic form of the catalytic cysteine,[96,97] hence preventing assumption of entirely analogous mechanism.

We observed that ecPGA, aPGA, and paPvdQ can accommodate for HSLs binding, stabilize HSLs in productive conformation, and can catalyze their degradation following equivalent reaction mechanisms. These mechanisms include geometrically comparable states at particular reaction steps, coherent with the currently established mechanism for ecPGA with its native substrate–penicillin G.[69] Energy barriers obtained from hundreds of replicated steered MD simulations for all investigated systems were in the vicinity of 10 kcal/mol and less which can be expected for this type of acylation reactions, in particular when considering the tendency of the utilized semi-empirical PM6-D method to underestimate them.[98] Using the same method, Nutho *et al.* showed that the barriers for acylation reaction catalyzed by Zika virus serine protease were ca. 8 kcal/mol lower than high-level QM/MM calculations.[99] Keeping this in mind, this would significantly lower the predicted acylation rates for both enzymes, resulting in worse rates when compared to their native substrates,[49,69] expected for substrates which were

not the primary ones. Furthermore, our computational inferences were supported by the experimental assays proving the activity of ecPGA and aPGA enzymes towards both C06-HSL and C08-HSL substrates and were in line with substrate preferences of paPvdQ available in the literature.[49] Catalytic efficiencies of ecPGA and aPGA calculated for studied substrates yielded k_{cat}/K_M values around 0.01 mM^{-1} s^{-1}, which was an order of magnitude lower than for kcPGA (0.11 mM^{-1} s^{-1}),[51] suggesting that although both enzymes exhibited basal activity towards short to medium length HSLs, kcPGA remains the more efficient one.

Importantly, our study indicates that paPvdQ, when compared to PGAs, more efficiently stabilizes HSLs in terms of productive binding, which is defined by a narrow and relatively static acyl-binding cavity limiting the mobility of the cleaved amide bond efficiently. Conversely, entrance to the acyl-binding cavity of PGAs is equipped with dynamic gates which enable these enzymes to accommodate a much broader range of substrates including HSL, various amino acids, and penicillins.[51,54,85,87] Our QM/MM MD-based study elucidated protein- and ligand-dependent differences in the dynamics of those gating residues, with a clear tendency of the aPGA to sample closed conformation with longer substrate compared to remaining PGAs complexes under study. This observation corresponds well with the insights from previous studies suggesting the preference for a closed state for free enzyme and complexes with specifically recognized ligands and an open state for nonspecific ligands.[53,91] Consequently, these gates and their structural proximity represent attractive engineering targets for further research aiming to develop PGA tailored against specific bacterial QS.

In summary, this study, conducted on three enzymes, members of two distinct protein sub-families of N-terminal serine hydrolases–penicillin G acylases and acyl-homoserine lactone acylases, elucidates common mechanisms of QQ activity towards HSLs, bacterial signaling molecules. Members of this family employ the same reaction mechanism to degrade QS compounds, with the several enzyme- as well as substrate-dependent determinants governing their respective efficiency. As such, the obtained results expand current insights into the overall enzymatic action of N-terminal serine hydrolases on a molecular level, to the best of our knowledge not shown for any of the proteins under study so far. Furthermore, we extend the set of known QQ enzymes by two members of industrially well-established and optimized enzymes–aPGA and ecPGA.[100–102] Finally, by the in-depth comparison of the structure-dynamics-function relationships of this QQ activity between paPvdQ and PGAs, we point out the potential limitations of PGAs in individual catalytic steps conditioning their relatively low activity, which constitute a further direction of the research and can result in the development of potent antibacterial agents.

ASSOCIATED CONTENT

Supplemetary information with the following content is available: multiple sequence alignment and sequence similarity matrix of investigated serine Ntn hydrolase family representatives; detailed computational protocol description; evolution of backbone RMSD plots for MD simulations; time evolution of the entrance bottleneck to the acyl-binding site; acyl-binding site dynamics; PCA states characterization; detailed characterization of docked HSL poses; inspection of ligands in productive conformations throughout MD trajectories; ligand RMSD plots for MD simulations; MM/GBSA binding energies per residue decomposition; characterization of favorable organization of protein-HSL complex suitable for the reaction; QM/MM MD sampling description; characterization of the active site geometries at particular stages of the reaction from QM/MM MD; energetics of the acylation reaction steps; evolution of RC components during the acylation reaction; experimental measurements of the aPGA and ecPGA enzymes activity as a function of substrate concentration; definition of differences in gating dynamics among investigated systems; distributions of ligand bending in particular stages of the reaction; and presentation of different open/closed state preference for aPGA and ecPGA enzymes depending on the bound ligand

AUTHOR CONTRIBUTIONS

B.S. performed the computational analyses; M.G. performed experimental characterization of ecPGA and aPGA; A.P. and H.M. executed all the bacterial flask and fed-batch cultivation in bioreactor to produce enzymes; J.B. designed the project, analyzed and interpreted data. The manuscript was written through contributions of all authors. All authors have given approval to the final version of the manuscript.

ACKNOWLEDGMENT

ABBREVIATIONS

QS, quorum sensing; QQ, quorum quenching; HSL, N-acyl-homoserine lactone; QSI, quorum sensing inhibitor; paPvdQ, *Pseudomonas aeruginosa* acyl-homoserine lactone acylase; PGA, penicillin G acylase, kcPGA, *Kluyvera citrophila* PGA; ecPGA, *Escherichia coli* PGA; aPGA, *Achromobacter spp.* PGA; MD, molecular dynamics; RMSD, root-mean-square deviation; PCA, principal component analysis; MM/GBSA, Molecular Mechanics / Generalized Born Surface Area; QM/MM MD, Quantum Mechanics / Molecular Mechanics MD simulation; NPT, isothermal-isobaric ensemble; TI, tetrahedral intermediate; AE, acyl-enzyme; RC, reaction coordinate; LCOD, linear combination of distances; PMF, potential of mean force; HPLC, high-performance liquid chromatography; PC, principal component; RMSF, root-mean-square fluctuation; MC, Michaelis complex; TS1, transition state 1; TS2a, transition state 2a; TS2b, transition state 2b

REFERENCES

(1) Perros, M. A Sustainable Model for Antibiotics. *Science* **2015**, *347* (6226), 1062–1064. https://doi.org/10.1126/science.aaa3048.

(2) Rantala, M.; Huovinen, P.; Hölsö, K.; Lilas, A.; Kaartinen, L. Survey of Condition-Based Prescribing of Antimicrobial Drugs for Dogs at a Veterinary Teaching Hospital. *Veterinary Record* **2004**, *155* (9), 259–262. https://doi.org/10.1136/vr.155.9.259.

(3) Schwarz, S.; Kehrenberg, C.; Walsh, T. R. Use of Antimicrobial Agents in Veterinary Medicine and Food Animal Production. *International Journal of Antimicrobial Agents* **2001**, *17* (6), 431–437. https://doi.org/10.1016/S0924-8579(01)00297-7.

(4) Cabello, F. C. Heavy Use of Prophylactic Antibiotics in Aquaculture: A Growing Problem for Human and Animal Health and for the Environment. *Environmental Microbiology* **2006**, *8* (7), 1137–1144. https://doi.org/10.1111/j.1462-2920.2006.01054.x.

(5) Cabello, F. C.; Godfrey, H. P.; Buschmann, A. H.; Dölz, H. J. Aquaculture as yet Another Environmental Gateway to the Development and Globalisation of Antimicrobial Resistance. *The Lancet Infectious Diseases* **2016**, *16* (7), e127–e133. https://doi.org/10.1016/S1473-3099(16)00100-6.

(6) Blair, J. M. A.; Webber, M. A.; Baylay, A. J.; Ogbolu, D. O.; Piddock, L. J. V. Molecular Mechanisms of Antibiotic Resistance. *Nature Reviews Microbiology* **2015**, *13* (1), 42–51. https://doi.org/10.1038/nrmicro3380.

(7) Roope, L. S. J.; Smith, R. D.; Pouwels, K. B.; Buchanan, J.; Abel, L.; Eibich, P.; Butler, C. C.; Tan, P. S.; Walker, A. S.; Robotham, J. V.; Wordsworth, S. The Challenge of Antimicrobial Resistance: What Economics Can Contribute. *Science* **2019**, *364* (6435). https://doi.org/10.1126/science.aau4679.

(8) Hernando-Amado, S.; Coque, T. M.; Baquero, F.; Martínez, J. L. Defining and Combating Antibiotic Resistance from One Health and Global Health Perspectives. *Nature Microbiology* **2019**, *4* (9), 1432–1442. https://doi.org/10.1038/s41564-019-0503-9.

(9) Annunziato, G. Strategies to Overcome Antimicrobial Resistance (AMR) Making Use of Non-Essential Target Inhibitors: A Review. *International Journal of Molecular Sciences* **2019**, *20* (23), 5844. https://doi.org/10.3390/ijms20235844.

(10) Martin, M. J.; Thottathil, S. E.; Newman, T. B. Antibiotics Overuse in Animal Agriculture: A Call to Action for Health Care Providers. *Am J Public Health* **2015**, *105* (12), 2409–2410. https://doi.org/10.2105/AJPH.2015.302870.

(11) Manyi-Loh, C.; Mamphweli, S.; Meyer, E.; Okoh, A. Antibiotic Use in Agriculture and Its Consequential Resistance in Environmental Sources: Potential Public Health Implications. *Molecules* **2018**, *23* (4). https://doi.org/10.3390/molecules23040795.

(12) Holmes, A. H.; Moore, L. S. P.; Sundsfjord, A.; Steinbakk, M.; Regmi, S.; Karkey, A.; Guerin, P. J.; Piddock, L. J. V. Understanding the Mechanisms and Drivers of Antimicrobial Resistance. *The Lancet* **2016**, *387* (10014), 176–187. https://doi.org/10.1016/S0140-6736(15)00473-0.

(13) Crofts, T. S.; Gasparrini, A. J.; Dantas, G. Next-Generation Approaches to Understand and Combat the Antibiotic Resistome. *Nature Reviews Microbiology* **2017**, *15* (7), 422–434. https://doi.org/10.1038/nrmicro.2017.28.

(14) Wright, G. D. Antibiotic Resistance in the Environment: A Link to the Clinic? *Current Opinion in Microbiology* **2010**, *13* (5), 589–594. https://doi.org/10.1016/j.mib.2010.08.005.

(15) Vaz-Moreira, I.; Nunes, O. C.; Manaia, C. M. Bacterial Diversity and Antibiotic Resistance in Water Habitats: Searching the Links with the Human Microbiome. *FEMS Microbiology Reviews* **2014**, *38* (4), 761–778. https://doi.org/10.1111/1574-6976.12062.

(16) Baquero, F.; Martínez, J.-L.; Cantón, R. Antibiotics and Antibiotic Resistance in Water Environments. *Current Opinion in Biotechnology* **2008**, *19* (3), 260–265. https://doi.org/10.1016/j.copbio.2008.05.006.

(17) Allen, H. K.; Donato, J.; Wang, H. H.; Cloud-Hansen, K. A.; Davies, J.; Handelsman, J. Call of the Wild: Antibiotic Resistance Genes in Natural Environments. *Nature Reviews Microbiology* **2010**, *8* (4), 251–259. https://doi.org/10.1038/nrmicro2312.

(18) World Health Organization. *Antimicrobial Resistance: Global Report on Surveillance*; World Health Organization: Geneva, Switzerland, 2014.

(19) Andersson, D. I.; Hughes, D. Antibiotic Resistance and Its Cost: Is It Possible to Reverse Resistance? *Nature Reviews Microbiology* **2010**, *8* (4), 260–271. https://doi.org/10.1038/nrmicro2319.

(20) Clatworthy, A. E.; Pierson, E.; Hung, D. T. Targeting Virulence: A New Paradigm for Antimicrobial Therapy. *Nature Chemical Biology* **2007**, *3* (9), 541–548. https://doi.org/10.1038/nchembio.2007.24.

(21) Bush, K.; Courvalin, P.; Dantas, G.; Davies, J.; Eisenstein, B.; Huovinen, P.; Jacoby, G. A.; Kishony, R.; Kreiswirth, B. N.; Kutter, E.; Lerner, S. A.; Levy, S.; Lewis, K.; Lomovskaya, O.; Miller, J. H.; Mobashery, S.; Piddock, L. J. V.; Projan, S.; Thomas, C. M.; Tomasz, A.; Tulkens, P. M.; Walsh, T. R.; Watson, J. D.; Witkowski, J.; Witte, W.; Wright, G.; Yeh, P.; Zgurskaya, H. I. Tackling Antibiotic Resistance. *Nature Reviews Microbiology* **2011**, *9* (12), 894–896. https://doi.org/10.1038/nrmicro2693.

(22) Berendonk, T. U.; Manaia, C. M.; Merlin, C.; Fatta-Kassinos, D.; Cytryn, E.; Walsh, F.; Bürgmann, H.; Sørum, H.; Norström, M.; Pons, M.-N.; Kreuzinger, N.; Huovinen, P.; Stefani, S.; Schwartz, T.; Kisand, V.; Baquero, F.; Martinez, J. L. Tackling Antibiotic Resistance: The Environmental Framework. *Nature Reviews Microbiology* **2015**, *13* (5), 310–317. https://doi.org/10.1038/nrmicro3439.

(23) Boeckel, T. P. V.; Glennon, E. E.; Chen, D.; Gilbert, M.; Robinson, T. P.; Grenfell, B. T.; Levin, S. A.; Bonhoeffer, S.; Laxminarayan, R. Reducing Antimicrobial Use in Food Animals. *Science* **2017**, *357* (6358), 1350–1352. https://doi.org/10.1126/science.aao1495.

(24) Laxminarayan, R.; Sridhar, D.; Blaser, M.; Wang, M.; Woolhouse, M. Achieving Global Targets for Antimicrobial Resistance. *Science* **2016**, *353* (6302), 874–875. https://doi.org/10.1126/science.aaf9286.

(25) Brown, E. D.; Wright, G. D. Antibacterial Drug Discovery in the Resistance Era. *Nature* **2016**, *529* (7586), 336–343. https://doi.org/10.1038/nature17042.

(26) Lewis, K. Platforms for Antibiotic Discovery. *Nat Rev Drug Discov* **2013**, *12* (5), 371–387. https://doi.org/10.1038/nrd3975.

(27) Payne, D. J.; Gwynn, M. N.; Holmes, D. J.; Pompliano, D. L. Drugs for Bad Bugs: Confronting the Challenges of Antibacterial Discovery. *Nat Rev Drug Discov* **2007**, *6* (1), 29–40. https://doi.org/10.1038/nrd2201.

(28) Tommasi, R.; Brown, D. G.; Walkup, G. K.; Manchester, J. I.; Miller, A. A. ESKAPEing the Labyrinth of Antibacterial Discovery. *Nat Rev Drug Discov* **2015**, *14* (8), 529–542. https://doi.org/10.1038/nrd4572.

(29) Lewis, K. The Science of Antibiotic Discovery. *Cell* **2020**, *181* (1), 29–45. https://doi.org/10.1016/j.cell.2020.02.056.

(30) Alekshun, M. N.; Levy, S. B. Molecular Mechanisms of Antibacterial Multidrug Resistance. *Cell* **2007**, *128* (6), 1037–1050. https://doi.org/10.1016/j.cell.2007.03.004.

(31) Theuretzbacher, U.; Outterson, K.; Engel, A.; Karlén, A. The Global Preclinical Antibacterial Pipeline. *Nature Reviews Microbiology* **2020**, *18* (5), 275–285. https://doi.org/10.1038/s41579-019-0288-0.

(32) Rex, J. H.; Fernandez Lynch, H.; Cohen, I. G.; Darrow, J. J.; Outterson, K. Designing Development Programs for Non-Traditional Antibacterial Agents. *Nature Communications* **2019**, *10* (1), 3416. https://doi.org/10.1038/s41467-019-11303-9.

(33) Barlow, G. Clinical Challenges in Antimicrobial Resistance. *Nature Microbiology* **2018**, *3* (3), 258–260. https://doi.org/10.1038/s41564-018-0121-y.

(34) Shore, C. K.; Coukell, A. Roadmap for Antibiotic Discovery. *Nature Microbiology* **2016**, *1* (6), 1–2. https://doi.org/10.1038/nmicrobiol.2016.83.

(35) Theuretzbacher, U.; Piddock, L. J. V. Non-Traditional Antibacterial Therapeutic Options and Challenges. *Cell Host & Microbe* **2019**, *26* (1), 61–72. https://doi.org/10.1016/j.chom.2019.06.004.

(36) Grandclément, C.; Tannières, M.; Moréra, S.; Dessaux, Y.; Faure, D. Quorum Quenching: Role in Nature and Applied Developments. *FEMS Microbiol Rev* **2016**, *40* (1), 86–116. https://doi.org/10.1093/femsre/fuv038.

(37) Utari, P. D.; Vogel, J.; Quax, W. J. Deciphering Physiological Functions of AHL Quorum Quenching Acylases. *Front. Microbiol.* **2017**, *8*. https://doi.org/10.3389/fmicb.2017.01123.

(38) Withers, H.; Swift, S.; Williams, P. Quorum Sensing as an Integral Component of Gene Regulatory Networks in Gram-Negative Bacteria. *Current Opinion in Microbiology* **2001**, *4* (2), 186–193. https://doi.org/10.1016/S1369-5274(00)00187-9.

(39) Murugayah, S. A.; Gerth, M. L. Engineering Quorum Quenching Enzymes: Progress and Perspectives. *Biochem. Soc. Trans.* **2019**, *47* (3), 793–800. https://doi.org/10.1042/BST20180165.

(40) Utari, P. D.; Setroikromo, R.; Melgert, B. N.; Quax, W. J. PvdQ Quorum Quenching Acylase Attenuates Pseudomonas Aeruginosa Virulence in a Mouse Model of Pulmonary Infection. *Front Cell Infect Microbiol* **2018**, *8*. https://doi.org/10.3389/fcimb.2018.00119.

(41) Fetzner, S. Quorum Quenching Enzymes. *Journal of Biotechnology* **2015**, *201*, 2–14. https://doi.org/10.1016/j.jbiotec.2014.09.001.

(42) Theuretzbacher, U.; Bush, K.; Harbarth, S.; Paul, M.; Rex, J. H.; Tacconelli, E.; Thwaites, G. E. Critical Analysis of Antibacterial Agents in Clinical Development. *Nature Reviews Microbiology* **2020**, *18* (5), 286–298. https://doi.org/10.1038/s41579-020-0340-0.

(43) Defoirdt, T. Quorum-Sensing Systems as Targets for Antivirulence Therapy. *Trends in Microbiology* **2018**, *26* (4), 313–328. https://doi.org/10.1016/j.tim.2017.10.005.

(44) Maeda, T.; García-Contreras, R.; Pu, M.; Sheng, L.; Garcia, L. R.; Tomás, M.; Wood, T. K. Quorum Quenching Quandary: Resistance to Antivirulence Compounds. *The ISME Journal* **2012**, *6* (3), 493–501. https://doi.org/10.1038/ismej.2011.122.

(45) Kalia, V. C.; Patel, S. K. S.; Kang, Y. C.; Lee, J.-K. Quorum Sensing Inhibitors as Antipathogens: Biotechnological Applications. *Biotechnology Advances* **2019**, *37* (1), 68–90. https://doi.org/10.1016/j.biotechadv.2018.11.006.

(46) Fuqua, C.; Parsek, M. R.; Greenberg, E. P. Regulation of Gene Expression by Cell-to-Cell Communication: Acyl-Homoserine Lactone Quorum Sensing. *Annu. Rev. Genet.* **2001**, *35* (1), 439–468. https://doi.org/10.1146/annurev.genet.35.102401.090913.

(47) Billot, R.; Plener, L.; Jacquet, P.; Elias, M.; Chabrière, E.; Daudé, D. Engineering Acyl-Homoserine Lactone-Interfering Enzymes toward Bacterial Control. *J. Biol. Chem.* **2020**, *295* (37), 12993–13007. https://doi.org/10.1074/jbc.REV120.013531.

(48) Bokhove, M.; Jimenez, P. N.; Quax, W. J.; Dijkstra, B. W. The Quorum-Quenching N-Acyl Homoserine Lactone Acylase PvdQ Is an Ntn-Hydrolase with an Unusual Substrate-Binding Pocket. *Proceedings of the National Academy of Sciences* **2010**, *107* (2), 686–691. https://doi.org/10.1073/pnas.0911839107.

(49) Koch, G.; Nadal-Jimenez, P.; Reis, C. R.; Muntendam, R.; Bokhove, M.; Melillo, E.; Dijkstra, B. W.; Cool, R. H.; Quax, W. J. Reducing Virulence of the Human Pathogen Burkholderia by Altering the Substrate Specificity of the Quorum-Quenching Acylase PvdQ. *Proceedings of the National Academy of Sciences* **2014**, *111* (4), 1568–1573. https://doi.org/10.1073/pnas.1311263111.

(50) Wahjudi, M.; Murugappan, S.; van Merkerk, R.; Eissens, A. C.; Visser, M. R.; Hinrichs, W. L. J.; Quax, W. J. Development of a Dry, Stable and Inhalable Acyl–Homoserine–Lactone–Acylase Powder Formulation for the Treatment of Pulmonary Pseudomonas Aeruginosa Infections. *European Journal of Pharmaceutical Sciences* **2013**, *48* (4–5), 637–643. https://doi.org/10.1016/j.ejps.2012.12.015.

(51) Mukherji, R.; Varshney, N. K.; Panigrahi, P.; Suresh, C. G.; Prabhune, A. A New Role for Penicillin Acylases: Degradation of Acyl Homoserine Lactone Quorum Sensing Signals by Kluyvera Citrophila Penicillin G Acylase. *Enzyme and Microbial Technology* **2014**, *56*, 1–7. https://doi.org/10.1016/j.enzmictec.2013.12.010.

(52) Lin, Y.-H.; Xu, J.-L.; Hu, J.; Wang, L.-H.; Ong, S. L.; Leadbetter, J. R.; Zhang, L.-H. Acyl-Homoserine Lactone Acylase from Ralstonia Strain XJ12B Represents a Novel and Potent Class of Quorum-Quenching Enzymes: Quorum-Quenching AHL-Acylase. *Molecular Microbiology* **2003**, *47* (3), 849–860. https://doi.org/10.1046/j.1365-2958.2003.03351.x.

(53) Novikov, F. N.; Stroganov, O. V.; Khaliullin, I. G.; Panin, N. V.; Shapovalova, I. V.; Chilov, G. G.; Švedas, V. K. Molecular Modeling of Different Substrate-Binding Modes and Their Role in Penicillin Acylase Catalysis. *The FEBS Journal* **2013**, *280* (1), 115–126. https://doi.org/10.1111/febs.12054.

(54) Alkema, W. B. L.; Dijkhuis, A.-J.; de Vries, E.; Janssen, D. B. The Role of Hydrophobic Active-Site Residues in Substrate Specificity and Acyl Transfer Activity of Penicillin Acylase: Role of Active-Site Phenylalanines in Penicillin Acylase. *European Journal of Biochemistry* **2002**, *269* (8), 2093–2100. https://doi.org/10.1046/j.1432-1033.2002.02857.x.

(55) McVey, C. E.; Walsh, M. A.; Dodson, G. G.; Wilson, K. S.; Brannigan, J. A. Crystal Structures of Penicillin Acylase Enzyme-Substrate Complexes: Structural Insights into the Catalytic Mechanism11Edited by K. Nagai. *Journal of Molecular Biology* **2001**, *313* (1), 139–150. https://doi.org/10.1006/jmbi.2001.5043.

(56) Clevenger, K. D.; Wu, R.; Er, J. A. V.; Liu, D.; Fast, W. Rational Design of a Transition State Analogue with Picomolar Affinity for Pseudomonas Aeruginosa PvdQ, a Siderophore Biosynthetic Enzyme. *ACS Chem. Biol.* **2013**, *8* (10), 2192–2200. https://doi.org/10.1021/cb400345h.

(57) Grulich, M.; Brezovský, J.; ŠtĿpánek, V.; Palyzová, A.; Kyslíková, E.; Kyslík, P. Resolution of α/β-Amino Acids by Enantioselective Penicillin G Acylase from Achromobacter Sp . *Journal of Molecular Catalysis B: Enzymatic* **2015**, *122*, 240–247. https://doi.org/10.1016/j.molcatb.2015.09.008.

(58) Schymkowitz, J.; Borg, J.; Stricher, F.; Nys, R.; Rousseau, F.; Serrano, L. The FoldX Web Server: An Online Force Field. *Nucleic Acids Res* **2005**, *33* (suppl_2), W382–W388. https://doi.org/10.1093/nar/gki387.

(59) Gordon, J. C.; Myers, J. B.; Folta, T.; Shoja, V.; Heath, L. S.; Onufriev, A. H++: A Server for Estimating p Ka s and Adding Missing Hydrogens to Macromolecules. *Nucleic Acids Res* **2005**, *33* (suppl_2), W368–W371. https://doi.org/10.1093/nar/gki464.

(60) Myers, J.; Grothaus, G.; Narayanan, S.; Onufriev, A. A Simple Clustering Algorithm Can Be Accurate Enough for Use in Calculations of PKs in Macromolecules. *Proteins: Structure, Function, and Bioinformatics* **2006**, *63* (4), 928–938. https://doi.org/10.1002/prot.20922.

(61) Anandakrishnan, R.; Aguilar, B.; Onufriev, A. V. H++ 3.0: Automating PK Prediction and the Preparation of Biomolecular Structures for Atomistic Molecular Modeling and Simulations. *Nucleic Acids Research* **2012**, *40* (W1), W537–W541. https://doi.org/10.1093/nar/gks375.

(62) D.A. Case; H.M. Aktulga; K. Belfon; I.Y. Ben-Shalom; S.R. Brozell; D.S. Cerutti; T.E. Cheatham; III, V.W.D. Cruzeiro, T.A. Darden, R.E. Duke, G. Giambasu, M.K. Gilson, H. Gohlke, A.W. Goetz, R. Harris, S. Izadi, S.A. Izmailov, C. Jin, K. Kasavajhala, M.C. Kaymak, E. King, A. Kovalenko, T. Kurtzman, T.S. Lee, S. LeGrand, P. Li, C. Lin, J. Liu, T. Luchko, R. Luo, M. Machado, V. Man, M. Manathunga, K.M. Merz, Y. Miao, O. Mikhailovskii, G. Monard, H. Nguyen, K.A. O'Hearn, A. Onufriev, F. Pan, S. Pantano, R. Qi, A. Rahnamoun, D.R. Roe, A. Roitberg, C. Sagui, S. Schott-Verdugo, J. Shen, C.L. Simmerling, N.R. Skrynnikov, J. Smith, J. Swails, R.C. Walker, J. Wang, H. Wei, R.M. Wolf, X. Wu, Y. Xue, D.M. York, S. Zhao, and P.A. Kollman. *AMBER 18*; University of California, San Francisco.

(63) Hopkins, C. W.; Le Grand, S.; Walker, R. C.; Roitberg, A. E. Long-Time-Step Molecular Dynamics through Hydrogen Mass Repartitioning. *J. Chem. Theory Comput.* **2015**, *11* (4), 1864–1874. https://doi.org/10.1021/ct5010406.

(64) Ryckaert, J.-P.; Ciccotti, G.; Berendsen, H. J. C. Numerical Integration of the Cartesian Equations of Motion of a System with Constraints: Molecular Dynamics of n-Alkanes. *Journal of Computational Physics* **1977**, *23* (3), 327–341. https://doi.org/10.1016/0021-9991(77)90098-5.

(65) Maier, J. A.; Martinez, C.; Kasavajhala, K.; Wickstrom, L.; Hauser, K. E.; Simmerling, C. Ff14SB: Improving the Accuracy of Protein Side Chain and Backbone Parameters from Ff99SB. *J. Chem. Theory Comput.* **2015**, *11* (8), 3696–3713. https://doi.org/10.1021/acs.jctc.5b00255.

(66) Zwanzig, R. Nonlinear Generalized Langevin Equations. *J Stat Phys* **1973**, *9* (3), 215–220. https://doi.org/10.1007/BF01008729.

(67) Pavelka, A.; Sebestova, E.; Kozlikova, B.; Brezovsky, J.; Sochor, J.; Damborsky, J. CAVER: Algorithms for Analyzing Dynamics of Tunnels in Macromolecules. *IEEE/ACM Transactions on Computational Biology and Bioinformatics* **2016**, *13* (3), 505–517. https://doi.org/10.1109/TCBB.2015.2459680.

(68) Pedregosa, F.; Varoquaux, G.; Gramfort, A.; Michel, V.; Thirion, B.; Grisel, O.; Blondel, M.; Prettenhofer, P.; Weiss, R.; Dubourg, V.; Vanderplas, J.; Passos, A.; Cournapeau, D.; Brucher, M.; Perrot, M.; Duchesnay, É. Scikit-Learn: Machine Learning in Python. *Journal of Machine Learning Research* **2011**, *12* (85), 2825–2830.

(69) Grigorenko, B. L.; Khrenova, M. G.; Nilov, D. K.; Nemukhin, A. V.; Švedas, V. K. Catalytic Cycle of Penicillin Acylase from *Escherichia Coli* : QM/MM Modeling of Chemical Transformations in the Enzyme Active Site upon Penicillin G Hydrolysis. *ACS Catal.* **2014**, *4* (8), 2521–2529. https://doi.org/10.1021/cs5002898.

(70) Zhiryakova, D.; Ivanov, I.; Ilieva, S.; Guncheva, M.; Galunsky, B.; Stambolieva, N. Do N-Terminal Nucleophile Hydrolases Indeed Have a Single Amino Acid Catalytic Center? *FEBS Journal* **2009**, *276* (9), 2589–2598. https://doi.org/10.1111/j.1742-4658.2009.06987.x.

(71) Morris, G. M.; Huey, R.; Lindstrom, W.; Sanner, M. F.; Belew, R. K.; Goodsell, D. S.; Olson, A. J. AutoDock4 and AutoDockTools4: Automated Docking with Selective Receptor Flexibility. *Journal of Computational Chemistry* **2009**, *30* (16), 2785–2791. https://doi.org/10.1002/jcc.21256.

(72) Daniel, L.; Buryska, T.; Prokop, Z.; Damborsky, J.; Brezovsky, J. Mechanism-Based Discovery of Novel Substrates of Haloalkane Dehalogenases Using in Silico Screening. *J. Chem. Inf. Model.* **2015**, *55* (1), 54–62. https://doi.org/10.1021/ci500486y.

(73) D.A. Case; I.Y. Ben-Shalom; S.R. Brozell; D.S. Cerutti; T.E. Cheatham; V.W.D. Cruzeiro; T.A. Darden; R.E. Duke; D. Ghoreishi; M.K. Gilson; H. Gohlke; A.W. Goetz, D. Greene,R Harris, N. Homeyer, Y. Huang,S. Izadi, A. Kovalenko, T. Kurtzman, T.S. Lee, S. LeGrand, P. Li, C. Lin, J. Liu, T. Luchko, R. Luo, D.J.Mermelstein, K.M. Merz, Y. Miao, G. Monard, C. Nguyen, H. Nguyen, I. Omelyan, A. Onufriev, F. Pan, R.Qi, D.R. Roe, A. Roitberg, C. Sagui, S. Schott-Verdugo, J. Shen, C.L. Simmerling, J. Smith, R. Salomon-Ferrer, J. Swails, R.C. Walker, J. Wang, H. Wei, R.M. Wolf, X. Wu, L. Xiao, D.M. York and P.A. Kollman. *AMBER 2018*; University of California, San Francisco, 2018.

(74) Miller, B. R.; McGee, T. D.; Swails, J. M.; Homeyer, N.; Gohlke, H.; Roitberg, A. E. MMPBSA.Py: An Efficient Program for End-State Free Energy Calculations. *J. Chem. Theory Comput.* **2012**, *8* (9), 3314–3321. https://doi.org/10.1021/ct300418h.

(75) Jindal, G.; Warshel, A. Exploring the Dependence of QM/MM Calculations of Enzyme Catalysis on the Size of the QM Region. *J. Phys. Chem. B* **2016**, *120* (37), 9913–9921. https://doi.org/10.1021/acs.jpcb.6b07203.

(76) Dhoke, G. V.; Davari, M. D.; Schwaneberg, U.; Bocola, M. QM/MM Calculations Revealing the Resting and Catalytic States in Zinc-Dependent Medium-Chain Dehydrogenases/Reductases. *ACS Catal.* **2015**, *5* (6), 3207–3215. https://doi.org/10.1021/cs501524k.

(77) Korth, M.; Thiel, W. Benchmarking Semiempirical Methods for Thermochemistry, Kinetics, and Noncovalent Interactions: OMx Methods Are Almost As Accurate and Robust As DFT-GGA Methods for Organic Molecules. *J. Chem. Theory Comput.* **2011**, *7* (9), 2929–2936. https://doi.org/10.1021/ct200434a.

(78) Park, S.; Khalili-Araghi, F.; Tajkhorshid, E.; Schulten, K. Free Energy Calculation from Steered Molecular Dynamics Simulations Using Jarzynski's Equality. *The Journal of Chemical Physics* **2003**, *119* (6), 3559–3566. https://doi.org/10.1063/1.1590311.

(79) Kyslik, P.; Stepanek, V.; Hollerova, L.; Becka, S.; Rajasekar, V. W.; Anupama, D.; Plhackova, K.; Marsalek, J. DNA Sequence Encoding Penicillin Acylase, Novel Recombinant Recombinant DNA Constructs and Recombinant Microorganisms. 8039604, October 18, 2011.

(80) Sobotková, L.; Štěpánek, V.; Plháčková, K.; Kyslík, P. Development of a High-Expression System for Penicillin G Acylase Based on the Recombinant Escherichia Coli Strain RE3(PKA18). *Enzyme and Microbial Technology* **1996**, *19* (5), 389–397. https://doi.org/10.1016/S0141-0229(96)00052-X.

(81) Škrob, F.; Bečka, S.; Plháčková, K.; Fotopulosová, V.; Kyslík, P. Novel Penicillin G Acylase from Achromobacter Sp. CCM 4824. *Enzyme and Microbial Technology* **2003**, *32* (6), 738–744. https://doi.org/10.1016/S0141-0229(03)00036-X.

(82) Bečka, S.; Štěpánek, V.; Vyasarayani, R. W.; Grulich, M.; Maršálek, J.; Plháčková, K.; Dobišová, M.; Marešová, H.; Plačková, M.; Valešová, R.; Palyzová, A.; Datla, A.; Ashar, T. K.; Kyslík, P. Penicillin G Acylase from Achromobacter Sp. CCM 4824. *Appl Microbiol Biotechnol* **2014**, *98* (3), 1195–1203. https://doi.org/10.1007/s00253-013-4945-3.

(83) Kutzbach, C.; Rauenbusch, E. Preparation and General Properties of Crystalline Penicillin Acylase from Escherichia Coli ATCC 11 105. *Hoppe-Seyler's Z. Physiol. Chem.* **1974**, *355* (1), 45–53. https://doi.org/10.1515/bchm2.1974.355.1.45.

(84) Kaushik, S.; Marques, S. M.; Khirsariya, P.; Paruch, K.; Libichova, L.; Brezovsky, J.; Prokop, Z.; Chaloupkova, R.; Damborsky, J. Impact of the Access Tunnel Engineering on Catalysis Is Strictly Ligand-Specific. *The FEBS Journal* **2018**, *285* (8), 1456–1476. https://doi.org/10.1111/febs.14418.

(85) Grulich, M.; Brezovský, J.; Štěpánek, V.; Palyzová, A.; Marešová, H.; Zahradník, J.; Kyslíková, E.; Kyslík, P. In-Silico Driven Engineering of Enantioselectivity of a Penicillin G Acylase towards Active Pharmaceutical Ingredients. *Journal of Molecular Catalysis B: Enzymatic* **2016**, *133*, S53–S59. https://doi.org/10.1016/j.molcatb.2016.11.014.

(86) Duggleby, H. J.; Tolley, S. P.; Hill, C. P.; Dodson, E. J.; Dodson, G.; Moody, P. C. Penicillin Acylase Has a Single-Amino-Acid Catalytic Centre. *Nature* **1995**, *373* (6511), 264–268. https://doi.org/10.1038/373264a0.

(87) Alkema, W. B. L.; Vries, E. de; Floris, R.; Janssen, D. B. Kinetics of Enzyme Acylation and Deacylation in the Penicillin Acylase-Catalyzed Synthesis of β-Lactam Antibiotics. *European Journal of Biochemistry* **2003**, *270* (18), 3675–3683. https://doi.org/10.1046/j.1432-1033.2003.03728.x.

(88) Morillas, M.; Goble, M. L.; Virden, R. The Kinetics of Acylation and Deacylation of Penicillin Acylase from Escherichia Coli ATCC 11105 : Evidence for Lowered PKa Values of Groups near the Catalytic Centre. **1999**, 5.

(89) Li, J.; Lim, S. P.; Beer, D.; Patel, V.; Wen, D.; Tumanut, C.; Tully, D. C.; Williams, J. A.; Jiricek, J.; Priestle, J. P.; Harris, J. L.; Vasudevan, S. G. Functional Profiling of Recombinant NS3 Proteases from All Four Serotypes of Dengue Virus Using Tetrapeptide and Octapeptide Substrate Libraries. *J. Biol. Chem.* **2005**, *280* (31), 28766–28774. https://doi.org/10.1074/jbc.M500588200.

(90) Alkema, W. B. L.; Prins, A. K.; de VRIES, E.; Janssen, D. B. Role of AArg145 and BArg263 in the Active Site of Penicillin Acylase of Escherichia Coli. *Biochemical Journal* **2002**, *365* (1), 303–309. https://doi.org/10.1042/bj20011468.

(91) Done, S. H.; Brannigan, J. A.; Moody, P. C. E.; Hubbard, R. E. Ligand-Induced Conformational Change in Penicillin Acylase. 13.

(92) Sikdar, R.; Elias, M. Quorum Quenching Enzymes and Their Effects on Virulence, Biofilm, and Microbiomes: A Review of Recent Advances. *Expert Rev Anti Infect Ther* **2020**, *18* (12), 1221–1233. https://doi.org/10.1080/14787210.2020.1794815.

(93) Liu, Y.; Ebalunode, J. O.; Briggs, J. M. Insights into the Substrate Binding Specificity of Quorum-Quenching Acylase PvdQ. *Journal of Molecular Graphics and Modelling* **2019**, *88*, 104–120. https://doi.org/10.1016/j.jmgm.2019.01.006.

(94) Clevenger, K. D.; Wu, R.; Liu, D.; Fast, W. N-Alkylboronic Acid Inhibitors Reveal Determinants of Ligand Specificity in the Quorum-Quenching and Siderophore Biosynthetic Enzyme PvdQ. *Biochemistry* **2014**, *53* (42), 6679–6686. https://doi.org/10.1021/bi501086s.

(95) Chilov, G. G.; Sidorova, A. V.; Švedas, V. K. Quantum Chemical Studies of the Catalytic Mechanism of N-Terminal Nucleophile Hydrolase. *Biochemistry Moscow* **2007**, *72* (5), 495–500. https://doi.org/10.1134/S0006297907050057.

(96) Lodola, A.; Branduardi, D.; De Vivo, M.; Capoferri, L.; Mor, M.; Piomelli, D.; Cavalli, A. A Catalytic Mechanism for Cysteine N-Terminal Nucleophile Hydrolases, as Revealed by Free Energy Simulations. *PLoS ONE* **2012**, *7* (2), e32397. https://doi.org/10.1371/journal.pone.0032397.

(97) Scalvini, L.; Ghidini, A.; Lodola, A.; Callegari, D.; Rivara, S.; Piomelli, D.; Mor, M. N-Acylethanolamine Acid Amidase (NAAA): Mechanism of Palmitoylethanolamide Hydrolysis Revealed by Mechanistic Simulations. *ACS Catal.* **2020**, *10* (20), 11797–11813. https://doi.org/10.1021/acscatal.0c02903.

(98) Yilmazer, N. D.; Korth, M. Enhanced Semiempirical QM Methods for Biomolecular Interactions. *Computational and Structural Biotechnology Journal* **2015**, *13*, 169–175. https://doi.org/10.1016/j.csbj.2015.02.004.

(99) Nutho, B.; Mulholland, A. J.; Rungrotmongkol, T. Quantum Mechanics/Molecular Mechanics (QM/MM) Calculations Support a Concerted Reaction Mechanism for the Zika Virus NS2B/NS3 Serine Protease with Its Substrate. *J. Phys. Chem. B* **2019**, *123* (13), 2889–2903. https://doi.org/10.1021/acs.jpcb.9b02157.

(100) Grulich, M.; Štěpánek, V.; Kyslík, P. Perspectives and Industrial Potential of PGA Selectivity and Promiscuity. *Biotechnology Advances* **2013**, *31* (8), 1458–1472. https://doi.org/10.1016/j.biotechadv.2013.07.005.

(101) Marešová, H.; Palyzová, A.; Plačková, M.; Grulich, M.; Rajasekar, V. W.; Štěpánek, V.; Kyslíková, E.; Kyslík, P. Potential of Pichia Pastoris for the Production of Industrial Penicillin G Acylase. *Folia Microbiol* **2017**, *62* (5), 417–424. https://doi.org/10.1007/s12223-017-0512-0.

(102) Marešová, H.; Plačková, M.; Grulich, M.; Kyslík, P. Current State and Perspectives of Penicillin G Acylase-Based Biocatalyses. *Appl Microbiol Biotechnol* **2014**, *98* (7), 2867–2879. https://doi.org/10.1007/s00253-013-5492-7.